Synthesis and characterization of graphene oxide-modified Bi2WO6 and its use as photocatalyst

By

Xiaoyue Hu

A thesis submitted to the Faculty of Graduate and Postdoctoral Studies in partial fulfillment of the requirements for the M.A.Sc. degree in Chemical Engineering

Department of Chemical and Biological Engineering

Faculty of Engineering

University of Ottawa

Abstract

The control of environmental pollution, particularly in wastewater treatment, is one of the major concerns of the 21st century. Among the currently available pollution control technologies, photocatalysis is one of the most promising and efficient approaches to the reduction of pollutants. Graphene, a carbon nanomaterial with specific physical and chemical properties, has been reported as a promising potential new catalyst material in this field.

A Bi_2WO_6 photocatalyst modified with graphene oxide was synthesized in a two-step hydrothermal process. Compared with pure Bi_2WO_6, the modified photocatalyst with 1.2 wt% graphene oxide improved photoactivity during the degradation of rhodamine-B (RhB) dye pollutant, by facilitating the dissociation of photogenerated excitons, which in turn results in more O_2^- radicals.

XRD characterization showed that the modification of Bi_2WO_6 with graphene oxide does not affect its structure or morphology. The adsorption properties of graphene also contribute to the improvement of photoactivity. Other parameters such as catalyst dosage, temperature and solution pH are studied, with the aim to improve the efficiency of RhB removal.

Résumé

La réduction de pollution environnementale, en particulier durant le traitement d'eaux usagées, est l'une des grandes préoccupations du 21^{e} siècle. Parmi les technologies présentement disponibles, la photocatalyse s'est avérée très prometteuse, et l'une des plus efficaces pour la réduction de polluants. Le graphène, un nanomatériel à base de carbone ayant des propriétés physico-chimiques particulières, est particulièrement intéressant comme catalyseur dans ce domaine.

Un photocatalyseur à base de Bi_2WO_6 et modifié avec de l'oxyde de graphène fut synthétisé à l'aide d'un procédé hydrothermal à deux étapes. Lors de la dégradation de polluants à base de teintures, la photoactivité du photocatalyseur contenant 1.2 % par poids d'oxyde de graphène est plus haute que celle du Bi_2WO_6 pur, dû à la facilitation de la dissociation d'excitons photo-générés plus, qui mène à la génération de plus de radicaux O_2^-.

La caractérisation du Bi_2WO_6 par diffraction à rayon X démontre que sa modification par l'oxyde de graphène ne modifie pas sa structure ou sa morphologie. Les propriétés d'adsorption du graphène contribuent également à l'amélioration de l'activité du photocatalyseur. Pour ce projet de recherche, la rhodamine-B (RhB) est utilisée comme polluant. D'autres paramètres, notamment le dosage du catalyseur, la température, et le pH de la solution furent aussi étudiés, afin d'améliorer l'efficacité de dégradation du RhB.

Acknowledgement

Undertaking master's research at the University of Ottawa has been a memorable and meaningful learning experience for me. I cannot express how grateful I am to those who have helped me during this great journey. The following are a few people that have supported me in my academic life.

First, let me take this opportunity to express my sincere thanks to my supervisor, Dr. Jason Zhang, for giving me the opportunity to complete a master's degree in chemical engineering. I learned a lot under his supervision, and his support and advice helped me a lot over the course of my research.

Thanks are also extended to all the professors at the Department of Chemical Engineering for their guidance and assistance.

I must also mention our group's senior members, Joanne Gamage McEvoy and Gabriel Potvin, for their expertise and assistance, as well as Louis Tremblay for technical support.

Many thanks to my labmates Ran Rong, Xiangchao Meng and Hanna Qin for their assistance and friendship.

The technical staff of the Department of Material Characterization Core Center, who helped me with the characterization tests, should also be noted.

Last but not least, I wish to sincerely thank my parents, whose continuous attention and care have sustained me, as well as all of my friends, for their company and inspiration that helped me get through every situation.

Table of Contents

List of figures

List of Tables

Nomenclature

GO	Graphene Oxide
BWO	Bismuth Tungstate
RhB	Rhodamine B
CB	Conduction band
VB	Valence band
e^-/h^+	Electron and hole pairs
XRD	X-ray diffraction
XPS	X-ray Photoelectron Spectroscopy
SEM	Scanning Electron Microscopy
STEM	Scanning Transmission Electron Microscopy
UV-vis	Ultraviolet Visible

Chapter 1- Thesis Introduction

1.1 Background

The rapid developments in the field nanotechnology in the 21st century have created novel avenues of investigation in semiconductor photocatalytic technology, especially relating to the application in environmental and energy issues. Heterogeneous photocatalytic reactions occur under room temperature. Nano-semiconductor oxide acts as the carrier. This will be an ideal, a broad prospect for environmental pollution control based on visible light-induced irradiation for the unique properties of nanometer photocatalytic technology. Photocatalysis is an efficient way to degrade organic pollutant. The principles of photocatalysis are based on band theory and photocatalytic oxidization: pollutant molecules are channeled onto a semiconductor electrode and a separate inert electrode. The oxidation-redox reaction happens separately on these two electrodes to promote the production of electron-hole pairs which can lead the oxidation and degradation of pollutant molecules.

Titanium dioxide (TiO_2) nanoparticles are widely used in environmental pollution control, construction of solar cells, self-cleaning of glass or ceramic tile, elimination of malignant bacteria, and other fields. However, TiO_2 has a wide band gap, at 3.2 eV; it can only absorb ultraviolet light with wavelengths of 387.5 nm or less. Currently, this is a major obstacle preventing the application of TiO_2 in the catalytic degradation of pollutants.

Recently, bismuth tungstate (Bi_2WO_6) has been studied for its photocatalytic properties. Its efficiency at degrading organic pollutants, chemical stability, low toxicity, reusability,

and low cost makes it an important discovery in the search for the optimal photocatalyst. However, the compound has some limitations including photo-response region and the efficiency for separating electron-hole pairs. For improving photocatalytic activity, some approaches have been investigated. Firstly, surface area of Bi_2WO_6 is increased by different synthesis methods. Secondly, photo-response region of Bi_2WO_6 is increased using doping ions, transition metals or other semiconductors. Thirdly, photo-induced electrons are migrated to restrict the recombination of photogenerated electrons and holes. Together these three approaches will enhance Bi_2WO_6's response to visible light, resulting in greatly improving visible-light photocatalytic activity.

1.2 Objectives

The main objectives of this study are summarized as follows.

- To synthesize Bi_2WO_6 via a template-free hydrothermal method.
- To synthesize graphene oxide modified Bi_2WO_6 composites and test their photocatalytic activity for a model organic dye.
- To study the size, structure, morphology, optical absorption properties and composition of photocatalysts by XRD, XPS, SEM, STEM and UV-vis technologies.
- To study the influence of operational parameters (catalyst dosage, temperature and pH value, etc.) governing the photocatalytic degradation.

1.3 Thesis outline

This manuscript is based on the following details of each section of research, presented as separate chapters.

Chapter 1 introduces the background and objectives of this study.

Chapter 2 presents a literature review concerning Bi_2WO_6 as a photocatalyst for wastewater treatment and provides a theoretical basis for the use of graphene to improve Bi_2WO_6 catalytic activity.

Chapter 3 evaluates different Bi_2WO_6 and Graphene Oxide-Bi_2WO_6 synthesis methods; in addition, it describes the result of characterization tests.

Chapter 4 tests the optimal ratio for combining graphene oxide and Bi_2WO_6 for efficient catalysis; in addition, it describes factors influencing the photocatalytic activity of Graphene Oxide-Bi_2WO_6.

Chapter 5 summarizes the work done and makes recommendations for future research.

Chapter 2-Literature Review

2.1 Semiconductor Photocatalysis

The growing levels of environmental pollution and the human energy needs are seriously jeopardizing the sustainability of human economic and social development in the 21st century. Environmental pollution is an issue of common concern for all modern societies (Braslavsky et al., 1996). A wide variety of methods have been developed for the sterilization, decontamination, and restoration of polluted environments (Boleda et al., 2011). Out of these, the semiconductor photocatalysis process, uses solar energy to catalyze the mineralization of organic pollutants and the sterilization of bacteria. It is a promising "green" environmental method (Tryk et al., 2000). Semiconductor photocatalysis is the most likely means of using freely available sunlight to eliminate pollution. Unfortunately, the conventional TiO_2 photocatalyst possesses a wide bandgap (Eg = 3.2 eV), which means the photocatalysis only happens when the absorbed energy reaches 3.2 eV. High-semiconductor carrier composite rate can be used just under ultraviolet light, which only occupies 3%-5% of the total energy of natural light (Malato et al., 2006; Hashimoto et al., 2005). Thus, the utilization of ultraviolet light to drive catalysis is undesirable. However, visible spectrum light accounts for 43% of the energy of sunlight; therefore, the development of efficient, visible light responsive photocatalytic materials has attracted the attention of scientists around the world. Currently, already discovered oxidized or polymerized visible light responsive semiconductor photocatalysts include Bi_2O_3, $BiVO_4$, Bi_2MoO_6 (Tian et al., 2011). However, theses single-phase

catalysts have low-quantum efficiency, which makes them not ideal for photocatalytic performance and use in the field.

2.2 Crystal Structure of Bi_2WO_6

Bismuth tungstate (Bi_2WO_6) is the simplest Aurivillius-type oxide layered structure comprising a perovskite structure WO_6 sheet (Figure 1) (Fu et al., 2005). Studies show that the atomic orbital 6s of Bismuth and 2p of Oxygen form a hybrid valence band; orbital 5d of Tungsten forms the conduction band. There is a bandgap between the valence band and the conduction band (Fu et al., 2005), when the absorbed energy is equal to or greater than the bandgap (Eg = 2.8eV) (Tian et al., 2011), the valence band is excited to the conduction band while leaving the corresponding valence band holes (h^+). Excited state photo-generated electrons and photogenerated holes (e^-/h^+) with high activity have a strong tendency to lose electrons and migrate to the surface of the semiconductor material. The redox reaction occurs at the semiconductor surface. The catalyst directly oxidizes various organic compounds to CO_2, H_2O and other small inorganic molecules (Rajeshwar et al., 2008; Fu et al., 2005). Therefore, Bi_2WO_6-based photocatalytic materials can be potentially used in pollutant clean-up.

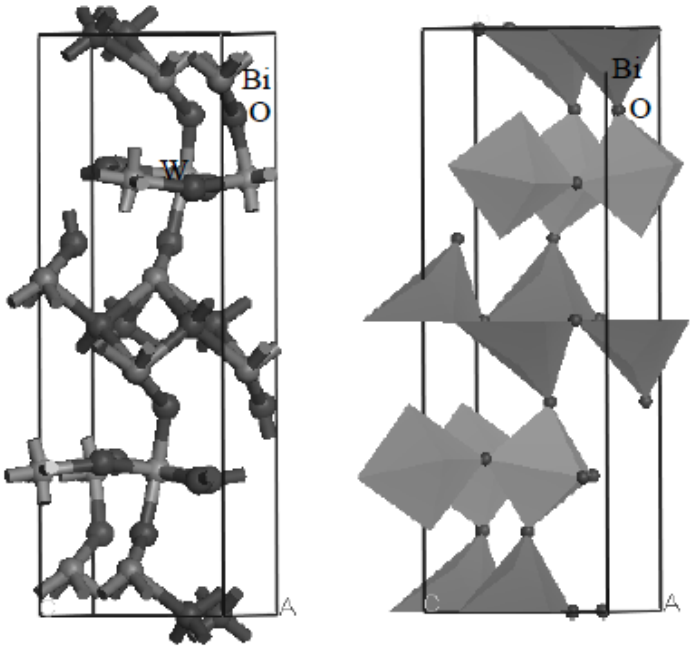

Figure 1- Crystal Structure of Bismuth Tungstate (Bi_2WO_6)

Adapted from (Fu et al., 2005)

2.3 The Photocatalytic Mechanism of Bi_2WO_6

Photocatalysis is based on the principle that upon irradiation of the photocatalyst with light, electrons are promoted from the valence band to the conduction band, which produces an electron-hole pair. This can be represented as follows:

$$Bi_2WO_6 + h\nu \rightarrow e^-_{CB} + h^+_{VB}$$

Where e^-_{cb} and h^+_{vb} are electrons in the conduction band and electrons vacancy in the valence band, respectively (Zhang et al., 2010). The electron-hole pair then rises to the surface of the catalyst, where a redox reaction will take place with chemicals found in the reaction vessel. The oxidative and reductive reactions are expressed as:

Oxidative reaction: $h^+ + \text{Organic} \rightarrow CO_2$

$$h^+ + H_2O \rightarrow \cdot OH + h^+$$

Reductive reaction: $\cdot OH + \text{Organic} \rightarrow CO_2$ (Hashimoto et al., 2005)

In the degradation of organic pollutants, a hydroxyl radical (OH·) is generated from the oxidation of a water molecule adsorbed onto the catalyst surface. This hydroxyl radical serves as the primary oxidant driving the reaction. But the presence of the oxygen in the hydroxyl group prevents the recombination of an electron–hole pair, which allows for further secondary reactions to occur (Fujishima et al., 1972).

During the photocatalytic reaction, when the reduction process of oxygen and the oxidation process of the pollutants do not advance simultaneously, there is also an accumulation of electrons, which causes an increase in the rate of recombination of e^- and h^+, eventually results in a decrease in catalytic efficiency. To forestall the drop off, many organic photodegradation catalysts utilize the oxidizing power of the holes either directly or indirectly to prevent the build-up of charge by offering a reducible species to react with and remove the electrons. Therefore, careful consideration for both oxidative and reductive paths is required when designing catalytic reactions (Peter et al., 1999).

Oxidizing species attack oxidizable contaminants to produce a step-wise break down of the contaminant molecules yielding CO_2, H_2O and final products. In order for this process to be commercialized, these following criteria must be satisfied:

a. The energy required to photo-excite the catalyst should be obtainable from normal sunlight (Malato et al., 2009).

b. The process should take place at ambient temperature and atmospheric pressure.

c. The oxidation of the pollutants to CO_2 and other inorganic products should be complete.

d. The oxygen needed for the reaction should be able to be directly obtained from the atmosphere.

e. The catalyst should have low toxicity.

f. The catalyst should be able to be reused.

g. The catalyst could be attached to different types of inert matrices for use in different environments and tasks.

The basic principles of this process are well established. A semiconductor can act as a sensitizer for light-induced redox process due to its electron structure, which is comprised of an electron-filled valence band and an empty conduction band. Absorption of a photon of energy that is greater than the band gap energy leads to the formation of an electron/hole pair (Chong et al., 2010).

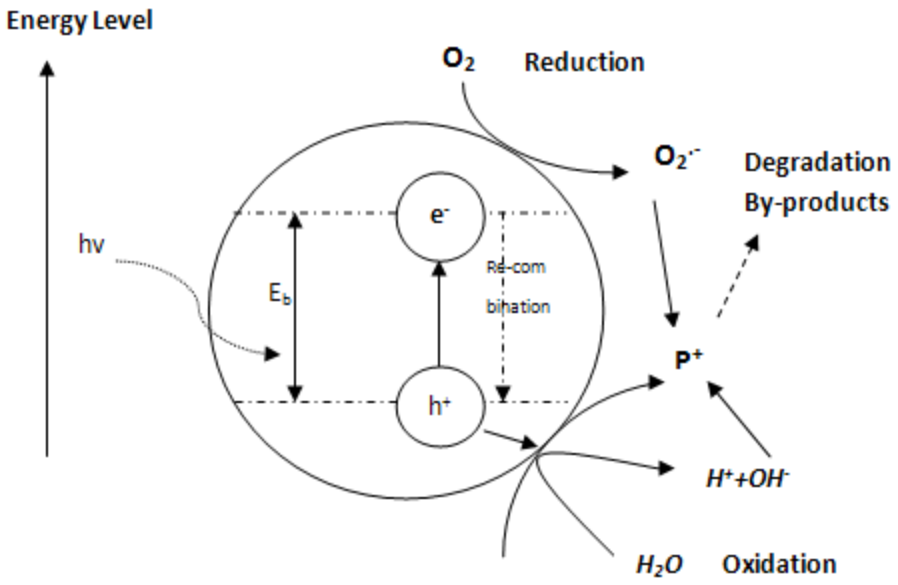

Figure 2- Photo-Induced Formation Mechanism of Electron Hole Pair in a Semiconductor Bi_2WO_6 Particle in the Presence of a Water Pollutant

Reproduced from (Chong et al., 2010) with permission from Elsevier

As the most representative semiconductor oxide, Bi_2WO_6 has been widely studied in the area of environmental pollution control and anti-bacterial/ anti-fouling coating material, etc. (Sun et al., 2011). In choosing a photocatalyst, the advantages of using Bi_2WO_6 are listed as follows:

a. The band gap energy of Bi_2WO_6 is 2.8 eV. The narrower band gap allows it to be activated by light of wavelengths of 385 nm and below (ultraviolet sunlight and fluorescent light) (Zhang et al., 2010), through modification, Bi_2WO_6 is expected to be able to use solar energy directly to induce the photocatalytic reaction.
b. It has high photocatalytic activity. The high potential of conduction band and valence band gives Bi_2WO_6 a strong oxidation-reduction ability. With it, most organic contaminants can be resolved.
c. It has excellent chemical stability and corrosion resistance.
d. It is relatively inexpensive, readily available and low-toxic.

Numerous studies have confirmed that the Bi_2WO_6 photocatalyst can effectively decompose dyes, organic halides, pesticides and other organics in water (Fu et al., 2005). When Bi_2WO_6 is loaded onto activated carbon, molecular sieve or other porous carriers, it can effectively degrade toxic organics in the air. In addition, when made into a thin film, Bi_2WO_6 demonstrates photo-induced hydrophilicity and light sterilization ability, which suggests many useful applications in healthcare, building materials and other fields.

2.4 Synthesis Method of Bi_2WO_6

Research on novel methods to synthesize Bi_2WO_6 has been developing over the years. Currently, validated synthesis protocols include the high-temperature solid-phase method, liquid precipitation method, ultrasonic synthesis method, hydrothermal method, solvothermal method, microwave hydrothermal method and microemulsion method (Sun et al., 2011; Zhang et al., 2010). These methods are briefly summarized below.

2.4.1 High-Temperature Solid-Phase Method

High-temperature solid-phase method is the most often used process for the preparation of Bi_2WO_6 powder. Bi_2O_3 and WO_3 are mixed at a molar ratio of 1:1 in ethanol, milled for several hours below 80℃ until completely dissolved. The mixture is dried and then calcined at 900℃ for 12 hours to produce Bi_2WO_6 powder (Tang et al., 2004). The study by Tang et al. found that Bi_2WO_6 thus prepared could degrade $CHCl_3$ and CH_3CHO to CO_2 in visible light. The advantages of the high-temperature solid-phase method are simple preparation procedure, high yield and low production cost. Disadvantages include high energy consumption, producing large particles (which have a smaller surface area, resulting in relatively lower photocatalytic activity).

2.4.2 Liquid Precipitation

The liquid precipitation method is based on the fact that bismuth nitrate that can dissolve in water, but when it reacts with sodium tungstate, the resulting Bi_2WO_6 is not water soluble and precipitates out. The precipitate is then filtered, washed, dried and calcined to obtain the Bi_2WO_6. Liquid phase precipitation was developed for the treatment of sugar refinery wastewater (Liu et al., 2005). Liu et al. had found that Bi_2WO_6 prepared using this method had better photocatalytic degradation performance compared to other tungstate catalysts and titanium dioxide. It also had better performance than Bi_2WO_6 prepared via the high-temperature solid-phase method. Bi_2WO_6 thus prepared was found to be relatively stable. Additives (Fe, Ti and Ce) reduced the degradation efficiency of co-catalyst Bi_2WO_6. Liquid phase precipitation is relatively easy to implement; the procedures are simple and does not require specialized equipment, but it requires baking at high temperatures in order to ensure high-quality crystalline products. High-temperature sintering will inevitably cause the formation of large particles, thus affecting the photocatalytic properties of powders.

2.4.3 Ultrasonic Synthesis

A recently discovered method for producing Bi_2WO_6 is ultrasonic synthesis. Aqueous $Bi(NO_3)_3 \cdot 5H_2O$ and $Na_2WO_4 \cdot 2H_2O$ are stirred together for 30min, sonicated for 60min, then the sonicated product is filtered, washed and calcined to isolate the Bi_2WO_6 photocatalyst (Zhou et al., 2007). When ultrasonic waves spread through a liquid, the

liquid particles are severely vibrated and made to interact strongly with each other. The dissolution rate of the solute and the rate of the chemical reactions are further accelerated by robust stirring. However, this protocol still requires high-temperature roasting, which would again inevitably cause agglomeration of the powder, and increasing the grain size, which would negatively impact the photocatalytic properties of powders.

2.4.4 Hydrothermal Method

Hydrothermal method requires a special closed reactor (i.e. autoclave). The reaction system is in aqueous solution and heated by pressurized vapour (or autogenous vapour pressure), creating a relatively high temperature and high-pressure reaction environment. Here, usually insoluble substances dissolve and recrystallize to form a solid-phase inorganic material.

Hydrothermal synthesis of Bi_2WO_6 powder is advantageous as it does not require high roasting temperatures and does not produce overly large particles. 5 mmol of $Bi(NO_3)_3 \cdot 5H_2O$ and 2.75 mmol $Na_2WO_4 \cdot 2H_2O$ were mixed in aqueous solution in a Teflon-lined autoclave tank (Amano et al., 2007). The reaction mixture was heated under high-vapour pressure for 20 hours to allow autogenous hydrothermal reaction to occur. The products were collected by filtration, centrifuged, washed with deionized distilled water, and dried at 120 ℃ to obtain flower sphere-like Bi_2WO_6. Fumiaki Amano et al. tested several reaction temperatures (130 ℃, 160 ℃, 190 ℃ and 220 ℃) to find out the best synthesize reacting temperature for the following degradation tests. 190 ℃ was determined to be the optimal reaction temperature. The resulting Bi_2WO_6 was able to

completely decomposed acetaldehyde into carbon dioxide, proving its high photocatalytic efficiency. Dekun Ma and colleagues (Ma et al., 2009) modified the above protocol, 1 mmol of $Bi(NO_3)_3 \cdot 5H_2O$ was added into an aqueous solution of 1 mmol citric acid to form a metal-citrate complex. The mixture was stirred vigorously for 10 minutes, then mixed with 0.5 mmol of $Na_2WO_4 \cdot 2H_2O$ and 2 mmol of $NaHCO_3$ and stirred for 5 minutes. The solution was then placed into a Teflon-lined autoclave and heated at 200 ℃ for 20 hours. The products were then centrifuged, washed and dried to obtain the three-dimensional self-assembled layered bismuth tungstate umbilical microspheres nanoparticles. Ma et al. tested the samples using BET, and the surface area of the powder was 2.41 m^2/g, 35 times greater compared with powders product via solid-phase method. The photocatalysts were assayed and showed good photocatalytic efficiency.

2.4.5 Solvothermal Method

The solvothermal method is a modification of the hydrothermal synthesis process where instead of using sole water as a medium, hot water containing an organic solvent is used. Chunxiao Xu and colleagues (Xu et al., 2009) chose ethylene glycol as a solvent. In their first experiment, 10 mmol of $Bi(NO_3)_3 \cdot 5H_2O$ was dissolved in 4.5 mL of 20 % v/v nitric acid, 5 mmol of Na_2WO_4 was dissolved in 40 mL of 60 % v/v ethylene glycol. Both solutions were vigorously stirred at room temperature for one hour. After adjusting the pH to 7.5 (using KOH), the resulting precursor suspensions were mixed in a polytetrafluoroethylene-lined tank reactor and heated at 180 ℃ for 2 hours. After cooling

to room temperature, washing and drying, Bi_2WO_6 powder obtained were compared to those produced via regular hydrothermal synthesis. The average grain size of synthesized Bi_2WO_6 nanocrystals was 12 nm, grains produced using the hydrothermal method had an average grain size of 53nm. Bi_2WO_6 nanocrystals prepared by the solvothermal method were able to degrade RhB: due to its smaller grain size and larger surface area, solvothermal Bi_2WO_6 nanocrystals resulted in better photocatalytic activity. However, a problem with this procedure is that $Bi(NO_3)_3 \cdot 5H_2O$ must be dissolved in concentrated nitric acid, and prolonged synthesis can corrode the reactor.

Using a modified procedure, Jian Zhu and colleagues (Zhu et al., 2009) dissolved $Bi(NO_3)_3 \cdot 5H_2O$ in a mixed solution of ethanol and glycerol (solution A). Simultaneously, $Na_2WO_4 \cdot 2H_2O$ was dissolved in a mixed solution of diethyl ether and glycerol (solution B). After magnetic stirring at room temperature, solution B was slowly added dropwise into the solution A forming a clear solution. The solution was stirred for a further 4 hours, and then transferred into an autoclave and heated at 110 ℃ for 20 hours. The product was then cooled to room temperature, washed with anhydrous ethanol and distilled deionized water, dried at 100 ℃ for 6 hours to obtain spherical Bi_2WO_6 powder. Activity tests showed that the powder was able to degrade RhB with high efficiency. The efficiency was three times higher than powers created using the hydrothermal method.

2.4.6 Microwave-Assisted Heating Method

The microwave-assisted heating method uses microwave heating as a way to combine the hydrothermal and solvothermal methods. Compared with previously described methods, the nano-powder and ceramic powder produced by the microwave-assisted heating method have faster response to the light source, shorter synthetic time, higher reaction efficiency, higher purity and narrower particle diameter distribution.

Ling Wu and colleagues (Wu et al., 2008) mixed $Bi(NO_3)_3 \cdot 5H_2O$: $Na_2WO_4 \cdot 2H_2O$ at a molar ratio of 2:1, the mixture was vigorously stirred and poured into an autoclave microwave reactor. The effects of different reaction temperatures, heating duration, and pH on Bi_2WO_6 synthesis were tested. The reaction temperature and time were found to be important factors affecting Bi_2WO_6 morphology. The study illustrated that the activity of the photocatalyst samples obtained through this procedure was much better than those produced via the solid-phase method.

Ling Wu and colleagues (Wu et al., 2008) synthesized Bi_2WO_6 powder using $Bi(NO_3)_3 \cdot 5H_2O$ and $(NH_4)_{10}W_{12}O_{41} \cdot 5H_2O$ as a starting material and ethylene glycol as a solvent. The pH of the mixture was adjusted to 9 with ammonia. The mixture was then heated in a microwave reactor at 160 ℃. Different heating durations (2 hour, 4 hour) were tested, and the 4-hour duration was found to produce optimal product. Compare with the traditional hydrothermal method, Bi_2WO_6 synthesized by the microwave solvothermal method has many advantages, including shorter integration time, higher specific surface area and more oxygen vacancies, which combines to produce higher photocatalytic efficiency.

2.4.7 Microemulsion Method

A microemulsion is produced when two immiscible solvents are mixed to form an emulsion under the action of a chemical surfactant, via micro-bubble nucleation, coalescence and agglomeration. Nanoparticles were then obtained after heat treatment. Lei Ge and colleagues (Ge et al., 2010) used Tween-80 as surfactant, n-butanol as co-surfactant, n-heptane as oil phase. Diluted nitric acid was added with stirring to dissolve the $Bi(NO_3)_3$ solution, and Na_2WO_4 was then added; lastly, Tween-80, n-butanol and n-heptane were added to the mixture. The pH of the mixture was adjusted to 7 using concentrated ammonia, and the mixture was heated in a reactor (multiple temperatures were tested). The products were washed and dried to obtain the Bi_2WO_6 photocatalyst. Visible light irradiation catalytic experiments showed that Bi_2WO_6 produced when heat treated at 170 ℃ samples have the highest photocatalytic activity.

2.4.8 Ultrasonic Spray Pyrolysis

Ultrasonic spray pyrolysis is a technique widely used in the synthesis of nanomaterial. Because all the powder particles are formed in the same solution, so a notable feature of ultrasonic spray pyrolysis is the uniform particle size of the product. Yu Huang and colleagues (Huang et al., 2010) dissolved citric acid and $Bi(NO_3)_3$ in concentrated

ammonia (solution A). Simultaneously, Na_2WO_4 was dissolved in concentrated ammonia (solution B). Solutions A and B were mixed and stirred for half an hour. The mixture is then diluted with distilled deionized water. The aqueous solution was atomized with a stream of air in an ultrasonic atomizer and blasted through a tube furnace. Droplets exiting the furnace were collected, and the products were filtered, centrifuged, washed with distilled deionized water and dried to obtain porous Bi_2WO_6 microspheres. The researchers found that reaction temperature is an important factor in controlling the morphology of the microspheres. Compared to the bulk powder Bi_2WO_6 produced by the solid state method, microsphere powder Bi_2WO_6 produced by the ultrasonic method had superior photocatalytic efficiency in removing NO_x.

2.5 Graphene in Improving the Photocatalytic Activity of Bi_2WO_6

The photocatalytic activity of Bi_2WO_6 is related to its intrinsic electric and conductive properties. Generally speaking, the photoactivity of Bi_2WO_6 is limited by the short duration of photogenerated electron-hole pairs and the optical absorption region of visible light. Because of this, it is necessary to modify Bi_2WO_6 to achieve catalytic efficiencies required for large-scale commercial applications (Gao et al., 2011). Recent studies have found two main ways to modify Bi_2WO_6. The first method is doping Bi_2WO_6 with other elements to narrow the band gap and simultaneously improve response to sunlight. (Tang et al., 2004) The second method is to modify the Bi_2WO_6 surface with other semiconductors or metal nanoparticles; this enhances its visible light photo-response

region and charge-transfer efficiency (Tang et al., 2004); simultaneously, this method suppresses electron-hole recombination to enhance photocatalytic activity.

Graphene modification of Bi_2WO_6 is based on the second method. This chapter will introduce the structure of graphene, its properties, and why graphene can improve the activity of precursor Bi_2WO_6 nanoparticles.

2.5.1 Introduction to Graphene

Graphene is one of the most hotly researched nanomaterials to date; it bears a great potential to improve the electrical property, mechanical property, thermal property and gas barrier property of polymer nanocomposites. Graphene is a single-sheet structure composed of carbon atoms. It consists of a hexagonal honeycomb lattice formed by sp^2 hybrid orbitals of carbon atoms (Novoselov et al., 2004). Graphene has been long considered a theoretical construct that cannot exist in real life (Novoselov et al., 2004). However, in 2004, Andrei Heim and Konstantin Novoselov at the University of Manchester successfully isolated graphene from graphite. For this ground-breaking work on graphene, Hein and Novoselov were awarded the 2010 Nobel Prize in Physics (Balandin et al., 2008).

Currently, graphene is the thinnest stable nanomaterial in the world (Frank et al., 2007). It is almost completely transparent, absorbing only 2.3% of the light shining through it. The thermal conductivity of graphene can reaches 5300 W/m·K (Frank et al., 2007), surpassing that of carbon nano-tubes and diamond. The electron mobility of graphene reach 15000 $cm^2/V{\cdot}s$ at room temperature, surpasses that of carbon nanotubes and monocrystalline silicon. The electrical resistivity of graphene is about 10^{-6} Ω·cm, which

makes it the lowest resistive material in the world, lower than copper or silver (Novoselov et al., 2004). Because of its low resistivity, and fast electron mobility, graphene could be used to develop thinner and faster electronic conductive elements and transistors. Furthermore, as graphene is transparent and a good conductor, it is also suitable for use in transparent touch screens, light boards and solar cells.

2.5.2 Structure of Graphene

Graphite (most commonly found in pencil lead) is composed of numerous near-carbon -atom-thick graphene sheets stacked in formation (Figure 3) (Mkhoyan et al., 2009). Before Geim and Novoselov, it was considered physically impossible for graphene to independently exist under natural conditions. But the experiments have proved that two-dimensional graphene crystals (surface monolayer of carbon atoms) indeed exist, and the thickness of a single-layer graphene is a single atomic layer of carbon atoms (Gmitra et al., 2009).

Carbon atoms in graphene are periodically arranged in the form of six-membered rings. Every and all carbon atoms are found in the same environment. Each carbon atom is connected to its three adjacent carbon atoms via the σ bond, which, through the S, P_x and P_y hybrid orbitals form covalent bonds, thus constituting a common sp^2 hybrid structure (Mkhoyan et al., 2009). The bond angles of this structure are uniformly 120^o. The mechanical properties of graphene can play an important role in maintaining the structural integrity of the sheet during the modification process. The carbon atoms' π electrons in the P_z orbital track form the electron cloud. π electrons can freely move

within the two-dimensional plane of a graphene sheet, which explains why graphene has good electrical conductivity (Gmitra et al., 2009). Intuitively, the carbon atoms in the graphene layer are arranged in a hexagonal honeycomb. Scientists used to consider this two-dimensional crystal thermodynamically unstable. Theoretical modelling showed that the melting point of graphite decreases as the number of the graphene layers stacked together (graphite film) decreases. When the film thickness reaches several layers the graphene will become very unstable, and it would roll into a cylindrical tube or simply break down (SekharáRout et al., 2008; Mkhoyan et al., 2009). Another reason is that due to the amplitude of atomic vibration, the carbon atoms will be seriously misaligned. Due to the size of the atoms, they would not be able to bond with each other; the distances between the bonding atoms are almost the same as the diameter of the carbon atoms, so a single-layer structure cannot be maintained. So why is a perfect two-dimensional crystal of graphene stable? The reason is that a graphene sheet is not flat, but undulate, which may explain why the graphene can exist in nature.

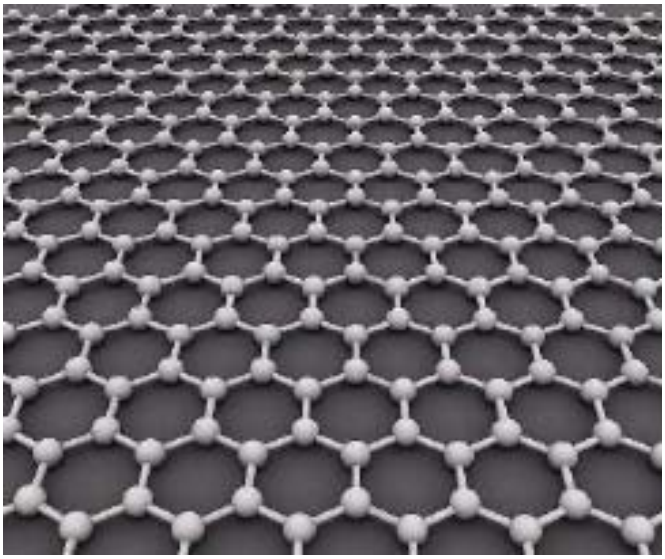

Figure 3-Structure of Graphene

Adapted from (SekharáRout et al., 2008)

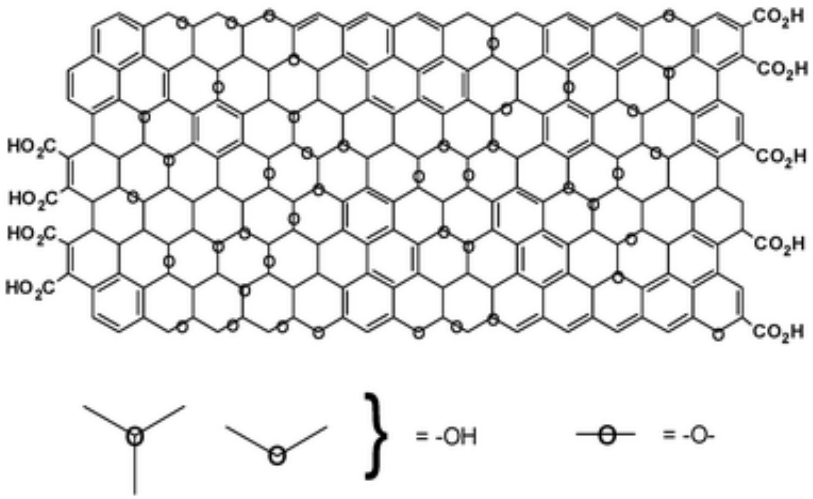

Figure 4-Structure of Graphene Oxide

Adapted from (Dreyer et al., 2010)

The structure of graphene oxide is similar to that of graphene, the only difference being the presence of a few function groups (i.e. –OH) attached to some of the carbons. The physical properties of graphene and graphene oxide are similar. However, the price for graphene oxide is much lower than that of graphene, so graphene oxide is used for modification instead of pure graphene. As the presence of the functional groups do not affect the optical property and conductive property of graphene oxide (compared to graphene).

2.5.3 Properties of Graphene

2.5.3.1 Electrical Property

As mentioned before, graphene has a unique electron structure, which gives its excellent electrical property. Graphene consists of a unit cell which contains two carbon atoms

(Potts et al., 2011). The corresponding Brillouin zone can be cross-banded. This structure is similar to a honeycomb structure of monolayer graphene in charge of transport and massless relativistic particles, which can be described as 2+1 form dimensional Dirac equation (Kim et al., 2010). Graphene is considered to be a zero-bandgap semiconductor. Thus, the carrier has a unique and special nature of the linear spectral characteristics. Graphene's special electron structure is dispersed in non-binding electronic parabolic way, which is not the same as the traditional metal and semiconductor.

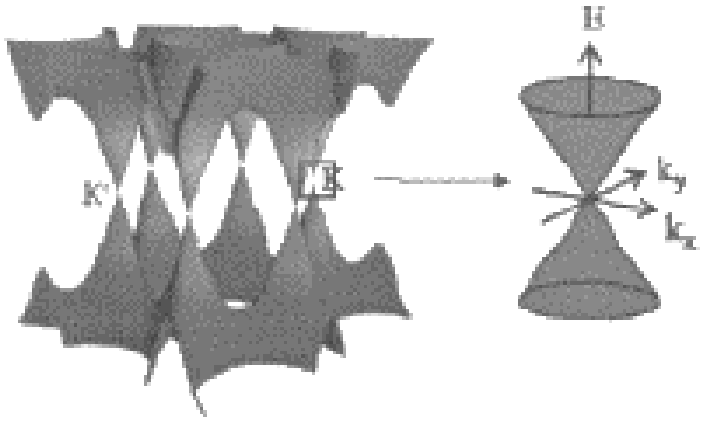

Figure 5- Electronic Structure of Single-Layer Graphene Schematic

Adapt from (Mkhoyan et al., 2009)

Graphene is traditionally defined as having ten carbon layers, or less, anything more than ten layers is termed graphite. At less than ten layers, graphene exhibits a different electron structure compared to graphite (Potts et al., 2011; Kim et al., 2010). Graphene possesses a bipolar field. Under certain conditions, the charge will be continuously tuned between electrons and holes. When a voltage is applied to the gate, and the electron mobility rate reaches 10000 $cm^2V^{-1}S^{-1}$ (Liu et al., 2008), an interesting phenomenon is observed. Ballistic transport properties of sub-micron level will appear. The ballistic transport distance is up to 0.3 μm at room temperature (Kim et al., 2010). The

phenomenon is minimally affected by temperature or doping effects. Graphene exhibit has a half-integer quantum Hall effect at low temperature. Its special band structure causes holes and electrons to separate from each other, leading to irregular quantum Hall effect (Stankovich et al., 2006). In a study of graphene electron spin, it is observed that electrons have two spin signals. The study concluded that the electrons' spin relaxation length do not depend on the current electron density of the graphene (Stankovich et al., 2006). Furthermore, two outer electrodes were placed on the graphene to study its superconducting properties, which was confirmed. Stable graphene lattice structure is responsible for its excellent conductivity, which is not affected by temperature (Liu et al., 2008).

2.5.3.2 Thermal Property

Theoretical studies have shown that graphene has excellent thermal performance (up to 3000 $W \cdot m^{-1}K^{-1}$) (Potts et al., 2011). Researchers at the University of California used confocal Raman microscopy in G-peak frequency and laser energy to determine that the thermal conductivity of graphene is within the range of $(4.54 \pm 0.44)\times10^3$ and $(5.30 \pm 0.45)\times10^3$ $W \cdot m^{-1}K^{-1}$ (Kim et al., 2010) at room temperature.

2.5.3.3 Mechanical Property

Graphene bonds consist of sp^2 hybrid orbitals, which gives the material its high mechanical strength (Rafiee et al., 2009). Graphene can withstand high levels of

externally applied mechanical forces. The surface carbon atoms are bent, thus allowing for the rearrangement of carbon atoms to maintain a stable structure. Experimentally measured, the stiffness of single-graphene layer is about 0.25 Tpa (Ramanathan et al., 2008). Lee and colleagues at Columbia University used atomic force microscopy to measure the microstructure of a graphene film according to its intrinsic strength (125 GPa) and elastic modulus (1100 GPa) (Lee et al., 2008). However in macroscopic materials, the presence of defects and grain boundaries affect the actual strength and modulus (Lee et al., 2008). The actual strength and elastic modulus would be lower.

2.5.3.4 Optical Property

Graphite is black, but graphene is almost completely transparent (Wakabayashi et al. 2008). A flawless graphene sheet can achieve more than 97% light transmission (Rafiee et al., 2009). The optical and conductive property of graphene are the two most important aspects to consider when modifying graphene for use in photocatalysts. Graphene is being researched for use in liquid crystal displays (LED), solar cells, optical equipments (Ramanathan et al., 2008) and as an aid for photocatalytic degradation of organic dyes.

2.5.3.5 Magnetic Property

The explanation of graphene's magnetic properties lies on the lone pair electrons in its serrated edge. After hydrogenated graphene single or dihydrotestosterone, its jag will become ferromagnetic (Ramanathan et al., 2008). Different methods to obtain graphene

effect are not the same. If the use of nano-diamond material was converted to graphene, Pauli paramagnetic susceptibility and spin paramagnetic susceptibility is better than 1-2 orders of magnitude higher than graphite. Experiments show that the nano-carbon fibers aligned with the three micro about graphene, treatment at different temperatures will have Cuire-Weiss characteristic, which indicates the local magnetic moments bit appears at the edge of the graphene (Wakabayashi et al. 2008). Additionally, graphene can be chemically modified in order to control its magnetic properties. Adsorbing oxygen onto the surface of graphene will increase its reluctance. Introducing potassium into the graphene will result in non-magnetic phenomenon occurring within the modified region.

2.5.4 Applications of Graphene in the Field of Photocatalysis

Previous studies have reported that increasing the separation efficiency of photogenerated carriers could significantly improve their photocatalytic performance (Gao et al., 2011). Graphene is a stable two-dimensional carbon nanomaterial which possesses excellent conductivity owing to its sp^2-bonded carbon network. Recently, photocatalysts have been created from graphene-modified semiconductor nanocomposites. The high transparency of graphene is a major impetus behind this avenue of research. The charge equilibration and electronic interaction between graphene and Bi_2WO_6 lead to a shift of the Fermi level and a decrease of the conduction band potential (Gao et al., 2011), which have an important influence on the photocatalytic process.

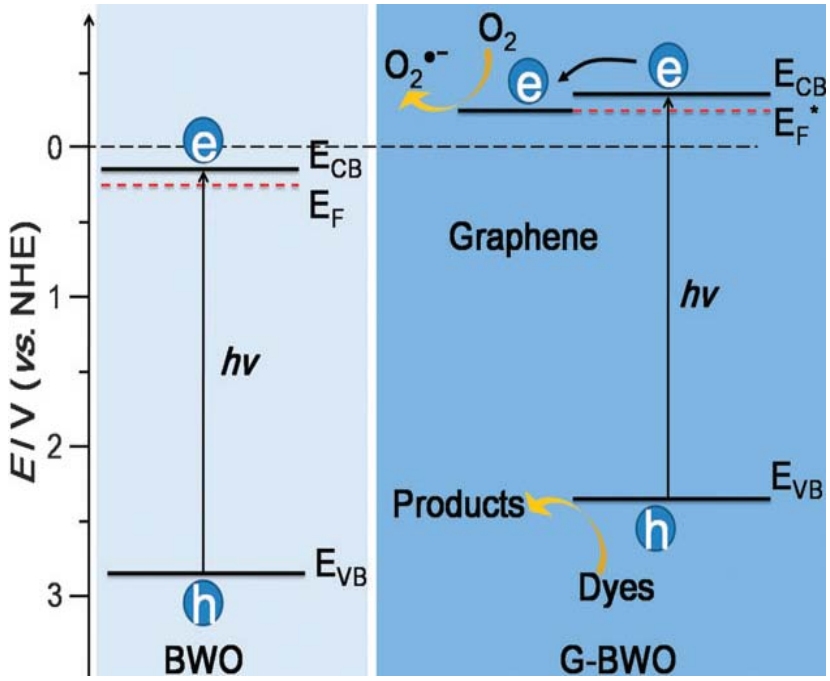

Figure 6- Schematic of Decreasing the Conduction Band Potential of Bi_2WO_6 by Graphene Adapt from (Gao et al., 2011)

2.6 Influence Parameters of Degradation Process

2.6.1 Morphology of Photocatalyst

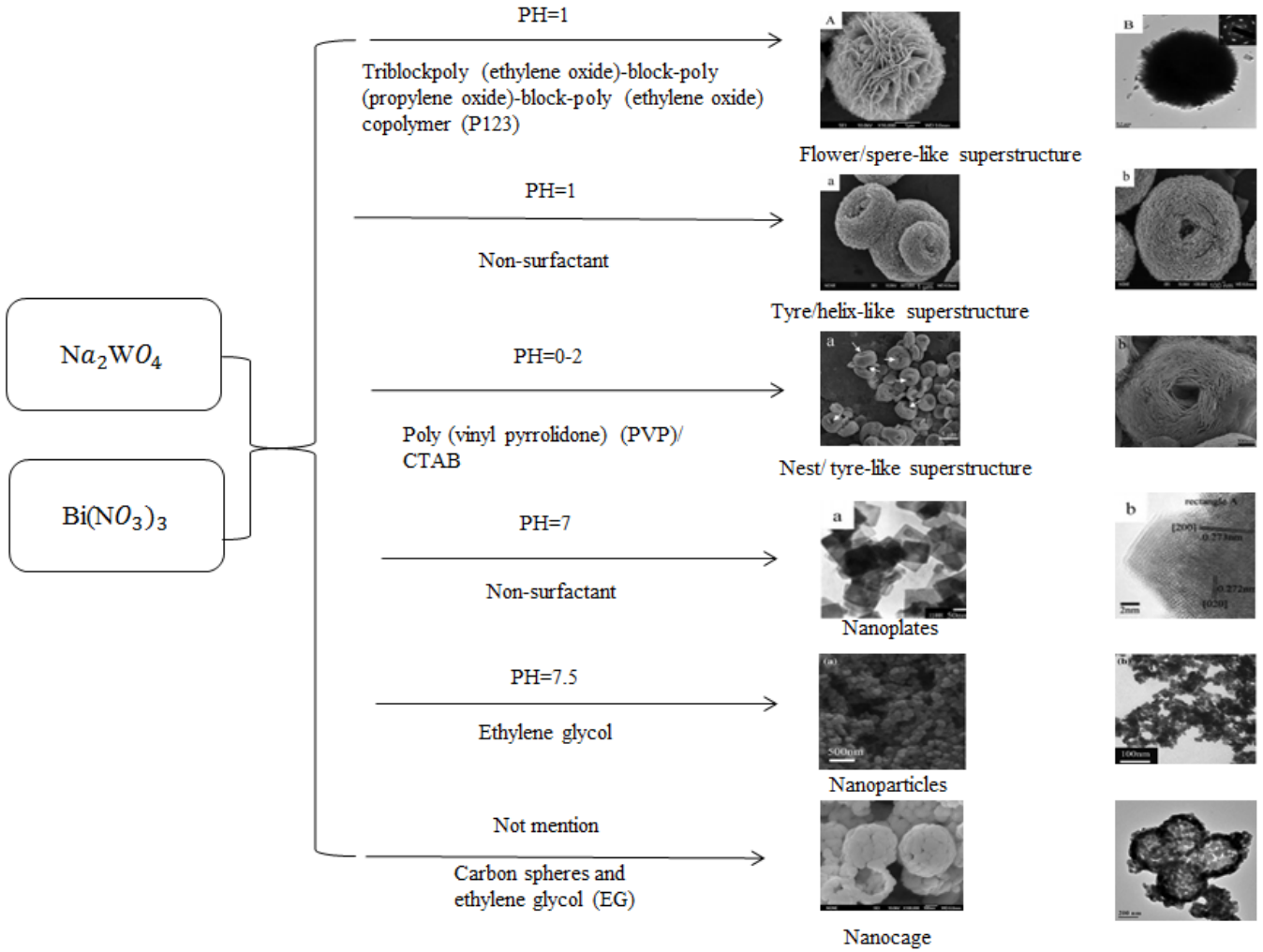

Figure 7- Bi_2WO_6 Morphologies Synthesized with Different pH Values with Different Surfactants

Adapt from (Zhang et al., 2009; Xu et al., 2005; Tian et al., 2011; Zhang et al., 2007; and Shang et al., 2008)

2.6.2 Catalyst Dosage

In a study by Zhang and colleagues, the initial rates of catalytic reaction were demonstrated to increase proportionally with the mass of catalyst (Zhang et al., 2007). However, when the mass of the catalyst exceeds a certain point, the reaction rate becomes independent of the mass. This is due to excess photocatalytic particles causing unfavorable light scattering effect and diminishing light penetration into the reaction solution, leading to a net decrease in photocatalytic activity as more catalyst is added (Tian et al., 2011). When designing real-life photocatalytic systems, the optimum mass of catalyst to be used must be determined to avoid excess catalyst dosage and ensure maximum photon absorption in order to achieve optimal reaction efficiency.

2.6.3 Initial pH Value

When photocatalytic reactions take place on semiconductor suspension in a pollutant solution, the reaction rate was shown to weakly correlate to pH of the solution (Zhang et al., 2007). Since the pH of the pollutant weakly affects the surface charge, particle size, size of formed aggregates and band edge positions of photocatalysts. The factor most strongly affected by pH is the catalyst's surface charge. The optimum pH value will mildly enhance the photodegradation efficiency of organic pollutants.

2.6.4 Temperature

Most photocatalytic reactions are not affected by minor variations in temperature. Most photocatalysis reactions can operate at room temperature, due to photonic activation (Zhang et al., 2009). The true activation energy (Et) is zero, while the apparent activation energy (Ea) is close to zero within the reaction temperature range of 20 ℃ to 80 ℃. When the reaction temperature is below 20℃ the activity decreases, as the energy is used in heating the catalyst instead of driving the reaction. When the reaction temperature increases to above 80 ℃, high temperature tends to cause recombination charge carriers and desorption of adsorbed reactant species. So the optimum reaction temperature is between 20 ℃ and 80 ℃ (Xu et al., 2005).

2.7 Applications of Bi_2WO_6 Photocatalysis Technology

Since the Industrial Revolution, our need for food, energy and manufactured goods have been rising at breakneck speeds. We, and the industries required to maintain our current standard of living are responsible for releasing a mindboggling amount of harmful pollutants into our environment. Examples include industrial wastewater and gases, pesticides, car exhaust, and toxic gases released from building materials (which not only threaten the environment-at-large, but also pose a more immediate danger on the human inhabitants of the building themselves). Traditional methods of pollution management and remediation such as chemical oxidation, microbial treatment,

high-temperature incineration, and physical adsorption have various shortcomings such as low efficiency (that can lead to the production of secondary pollution), narrow range of applications and high-energy consumption. However, Bi_2WO_6 photocatalytic technology is a high-efficiency and low-energy consumption method; it can be used to deal with a wide range of pollutants. Table 1 summarizes the recent research concerning the application of Bi_2WO_6 photocatalytic technology in the field of environmental pollution control and the degradation of toxic and hazardous pollutants.

Since the 2000s, Bi_2WO_6 has received widespread attention. Many companies, universities and government agencies have been actively working on the development and application of Bi_2WO_6 photocatalysts. Most of the work have been focused on urban environmental protection applications, such as incorporating them into city infrastructure (i.e. highway noise walls, street lights, road surfaces), other applications being investigated include decontaminating garbage disposal sites and treating waste water. Bi_2WO_6 can also be incorporated in more domestic market such as in automobile spray materials and building materials (to remove pollutants from living spaces).

Air pollution is made up of two primary components: organic gases and microorganisms. Most of the harmful organic gases are from paints (interior and exterior), adhesives, plywood, vinyl flooring, wallpaper and other construction/ furnishing materials, which release volatile organic compounds, such as formaldehyde, benzene, toluene and many other gases into the living space. The microorganisms in

the air are mainly composed of respiratory tract microorganisms breathed out by animals and humans, and bacteria and fungi sloughed off skin (such as mold). Conventional domestic air purifiers mainly use physical adsorption to remove indoor pollutants or use of negative ions such as ozone to remove harmful gases. Ultraviolet light is also used to sterilize the air (e.g. in biological safety cabinets), but these conventional methods have many limitations such as cannot directly use natural light, and long-term exposure can be harmful to the health.

Table 1- Photocatalytic Oxidation Technology Degradation of Toxic and Harmful Pollutants

Category	Name of Pollutants	Reference
Hydrocarbon	Octane	(Wang et al., 2006)
Phenol	Phenol	(Matos J. et al., 1998)
	Nitro phenol	(Loddo V. et al., 1999)
Aldehyde/Ketone	Acetone	(Choi W. Y. et al., 2001)
Alcohol	Methanol	(Iengo P. et al., 1999)
	Ethanol	(Pilkenton S. et al., 1999)
	2-Propanol	(Yamashita H. et al., 2000; Yamashita H. et al., 1998)
Carboxylic Acid and its Derivatives	Malic Acid	(Herrmann J-M. et al., 1999)
	Acetic Acid	(Roberto L. et al. ,1999; Peill N.J. et al., 1996)

	Sulphosalicylic Acid	(Ma et al., 1998)
	Stearic Acid	(P. Sawunyama et al., 1997)
Halide	Malachite Green ($C_{23}H_{25}N_2Cl$)	(Kominami H. et al., 2001)
	Pentachlorophenol	(Peill N.J. et al., 1996)
	4-Chlorine Phenol	(HerrmannJ-M. et al., 1994; Hofstadler K. et al., 1994)
	Dichloroacetic Acid	(Peill N.J. et al., 1996)
	Chlorinated Ethylene Phosphate	(Xiuru Y. et al., 2000)
	3,5-Dichloro-N-(1,1,-Dimethyl-2 Propyne)	(Takeda N. et al., 1998)
	Propyzamide	(Uchida H. et al., 1996)
Nitride	Methyl Orange	(Fengqing W. et al., 2000)
	Methylene Blue	(Yong T. et al., 2001)

2.8 Conclusion

The mechanism of action and applications of Bi_2WO_6 photocatalyst have been described above. Bi_2WO_6 is a visible light-induced photocatalytic material. It shows tremendous application potential in the field of pollutant degradation. Many features

make Bi_2WO_6 photocatalytic materials a natural fit the green, sustainable world of the future.

Thus, further investigations on the material are desperately needed to overcome the obstacles currently blocking the use of the photocatalyst in real life. The high rate of recombination for electron-hole pairs in the unmodified Bi_2WO_6 material restricts its application for photocatalysis. Considering the synergetic effect between the graphene oxide and semiconductor components, electron migration efficiency can be improved through the high-Schottky barrier at the interface of the graphene oxide and Bi_2WO_6 to facilitate the charge separation. A previous study (Zhang et al., 2009) showed some drawbacks reducing the reusability of Bi_2WO_6-assisted photocatalysts and limiting its ability to absorb visible light. Before this technology can enter the commercial arena, it is necessary to design novel and high-efficiency Bi_2WO_6-assisted photocatalysts. In the study (Zhang et al., 2009), graphene oxide coating on the surface of flak-ball Bi_2WO_6 superstructure has been synthesized by a template-free hydrothermal method. RhB was used as the experimental pollutant to evaluate the photocatalytic activity of the samples when under visible light irradiation. More work on elucidating the structure-property relationship of novel visible light-induced photocatalytic materials still have to be done before these materials are ready for large-scale applications.

2.9 References

Boleda, M. R., Galceran, M. T., & Ventura, F. (2011). Behavior of pharmaceuticals and drugs of abuse in a drinking water treatment plant (DWTP) using combined conventional and ultrafiltration and reverse osmosis (UF/RO) treatments. *Environmental Pollution*, *159*(6), 1584-1591.

Braslavsky, S. E., Houk, K. N., & Verhoeven, J. W. (1996). Glossary of terms used in photochemistry. *International Union of Pure and Applied Chemistry*.

Tryk, D. A., Fujishima, A., & Honda, K. (2000). Recent topics in photoelectrochemistry: achievements and future prospects. *Electrochimica acta*, *45*(15), 2363-2376.

Malato, S., Fernández-Ibáñez, P., Maldonado, M. I., Blanco, J., & Gernjak, W. (2009). Decontamination and disinfection of water by solar photocatalysis: recent overview and trends. *Catalysis Today*, *147*(1), 1-59.

Hashimoto, K., Irie, H., & Fujishima, A. (2005). TiO_2 photocatalysis: a historical overview and future prospects. *Japanese Journal of Applied Physics*, *44*(12R), 8269.

Tian, Y., Hua, G., Xu, W., Li, N., Fang, M., & Zhang, L. (2011). Bismuth tungstate nano/microstructures: Controllable morphologies, growth mechanism and photocatalytic properties. *Journal of Alloys and Compounds*, *509*(3), 724-730.

Fu, H., Pan, C., Yao, W., & Zhu, Y. (2005). Visible-light-induced degradation of rhodamine B by nanosized Bi_2WO_6. *The Journal of Physical Chemistry B*, *109*(47), 22432-22439.

Rajeshwar, K., Osugi, M. E., Chanmanee, W., Chenthamarakshan, C. R., Zanoni, M. V. B., Kajitvichyanukul, P., & Krishnan-Ayer, R. (2008). Heterogeneous photocatalytic treatment of organic dyes in air and aqueous media. *Journal of Photochemistry and Photobiology C: Photochemistry Reviews*, *9*(4), 171-192.

Zhang, Z., Wang, W., Shang, M., & Yin, W. (2010). Low-temperature combustion synthesis of Bi_2WO_6 nanoparticles as a visible-light-driven photocatalyst. *Journal of hazardous materials*, *177*(1), 1013-1018.

Fujishima, A. (1972). Electrochemical photolysis of water at a semiconductor electrode. *nature*, *238*, 37-38.

Peter, L. M. (1999). Applications of Kinetic Modeling. *Photoelectrochemical Kinetics at Semiconductor Electrodes*, 223.

Chong, M. N., Jin, B., Chow, C. W., & Saint, C. (2010). Recent developments in photocatalytic water treatment technology: a review. *Water research*, *44*(10), 2997-3027.

Sun, S., Wang, W., Xu, J., Wang, L., & Zhang, Z. (2011). Highly efficient photocatalytic oxidation of phenol over ordered mesoporous Bi_2WO_6. *Applied Catalysis B: Environmental*, *106*(3), 559-564.

Tang, J., Zou, Z., & Ye, J. (2004). Photocatalytic decomposition of organic contaminants by Bi_2WO_6 under visible light irradiation. *Catalysis Letters*, *92*(1-2), 53-56.

Liu, J. F., Peng, J. F., Chi, Y. G., & Jiang, G. B. (2005). Determination of formaldehyde in shiitake mushroom by ionic liquid-based liquid-phase microextraction coupled with liquid chromatography. *Talanta*, *65*(3), 705-709.

Zhou, L., Wang, W., & Zhang, L. (2007). Ultrasonic-assisted synthesis of visible-light-induced Bi_2MO_6 (M= W, Mo) photocatalysts. *Journal of Molecular Catalysis A: Chemical*, *268*(1), 195-200.

Amano, F., Nogami, K., Abe, R., & Ohtani, B. (2007). Facile hydrothermal preparation and photocatalytic activity of bismuth tungstate polycrystalline flake-ball particles. *Chemistry Letters*, *36*(11), 1314-1315.

Ma, D., Huang, S., Chen, W., Hu, S., Shi, F., & Fan, K. (2009). Self-assembled three-dimensional hierarchical umbilicate Bi_2WO_6 microspheres from nanoplates: controlled synthesis, photocatalytic activities and wettability. *The Journal of Physical Chemistry C*, *113*(11), 4369-4374.

Xu, C., Wei, X., Ren, Z., Wang, Y., Xu, G., Shen, G., & Han, G. (2009). Solvothermal preparation of Bi_2WO_6 nanocrystals with improved visible light photocatalytic activity. *Materials Letters*, *63*(26), 2194-2197.

Zhu, J., Wang, J. G., Bian, Z. F., Cao, F. G., & Li, H. X. (2009). Solvothermal synthesis of highly active Bi_2WO_6 visible photocatalyst. *Research on Chemical Intermediates*, *35*(6-7), 799-806.

Wu, L., Bi, J., Li, Z., Wang, X., & Fu, X. (2008). Rapid preparation of Bi_2WO_6 photocatalyst with nanosheet morphology via microwave-assisted solvothermal synthesis. *Catalysis Today*, *131*(1), 15-20.

Ge, L., & Zhang, X. (2010). Beijing 102249, China; Novel visible light driven Bi_2WO_6 photocatalysts synthesized via the microemulsion process and its photocatalytic performance [J]. *Journal of the Chinese Ceramic Society, 3*.

Huang, Y., Ai, Z., Ho, W., Chen, M., & Lee, S. (2010). Ultrasonic spray pyrolysis synthesis of porous Bi_2WO_6 microspheres and their visible-light-induced photocatalytic removal of NO. *The Journal of Physical Chemistry C,114*(14), 6342-6349.

Gao, E.,Wang, W., Shang, M., & Xu, J. (2011). Synthesis and enhanced photocatalytic performance of graphene-Bi_2WO_6 composite. *Physical Chemistry Chemical Physics, 13*(7), 2887-2893.

Novoselov, K. S., Geim, A. K., Morozov, S. V., Jiang, D., Zhang, Y., Dubonos, S. V. & Firsov, A. A. (2004). Electric field effect in atomically thin carbon films. *Science, 306*(5696), 666-669.

Balandin, A. A., Ghosh, S., Bao, W., Calizo, I., Teweldebrhan, D., Miao, F., & Lau, C. N. (2008). Superior thermal conductivity of single-layer graphene. *Nano letters, 8*(3), 902-907.

Frank, I. W., Tanenbaum, D. M., Van der Zande, A. M., & McEuen, P. L. (2007). Mechanical properties of suspended graphene sheets. *Journal of Vacuum Science & Technology B, 25*(6), 2558-2561.

Mkhoyan, K. A., Contryman, A. W., Silcox, J., Stewart, D. A., Eda, G., Mattevi, C. & Chhowalla, M. (2009). Atomic and electronic structure of graphene-oxide. *Nano Letters, 9*(3), 1058-1063.

Gmitra, M., Konschuh, S., Ertler, C., Ambrosch-Draxl, C., & Fabian, J. (2009). Band-structure topologies of graphene: spin-orbit coupling effects from first principles. *Physical Review B*, *80*(23), 235431.

SekharáRout, C. (2008). Changes in the electronic structure and properties of graphene induced by molecular charge-transfer. *Chemical Communications*, (41), 5155-5157.

Dreyer, D. R., Park, S., Bielawski, C. W., & Ruoff, R. S. (2010). The chemistry of graphene oxide. *Chemical Society Reviews*, 39(1), 228-240.

Potts, J. R., Dreyer, D. R., Bielawski, C. W., & Ruoff, R. S. (2011). Graphene-based polymer nanocomposites. *Polymer*, *52*(1), 5-25.

Kim, H., Abdala, A. A., & Macosko, C. W. (2010). Graphene/polymer nanocomposites. *Macromolecules*, *43*(16), 6515-6530.

Stankovich, S., Dikin, D. A., Dommett, G. H., Kohlhaas, K. M., Zimney, E. J., Stach, E. A. & Ruoff, R. S. (2006). Graphene-based composite materials. *Nature*, *442*(7100), 282-286.

Liu, N., Luo, F., Wu, H., Liu, Y., Zhang, C., & Chen, J. (2008). One-Step Ionic-Liquid-Assisted Electrochemical Synthesis of Ionic-Liquid-Functionalized Graphene Sheets Directly from Graphite. *Advanced Functional Materials*, *18*(10), 1518-1525.

Lee, C., Wei, X., Kysar, J. W., & Hone, J. (2008). Measurement of the elastic properties and intrinsic strength of monolayer graphene. *science*,*321*(5887), 385-388.

Gómez-Navarro, C., Sundaram, R. S., López, V., Zamora, F., Gómez-Herrero, J., Burghard, M., & Kern, K. Chemically derived graphene: electronic and mechanical properties.

Rafiee, M. A., Rafiee, J., Wang, Z., Song, H., Yu, Z. Z., & Koratkar, N. (2009). Enhanced mechanical properties of nanocomposites at low graphene content. *ACS nano*, *3*(12), 3884-3890.

Ramanathan, T., Abdala, A. A., Stankovich, S., Dikin, D. A., Herrera-Alonso, M., Piner, R. D. & Brinson, L. C. (2008). Functionalized graphene sheets for polymer nanocomposites. *Nature Nanotechnology*, *3*(6), 327-331.

Wakabayashi, K., Pierre, C., Dikin, D. A., Ruoff, R. S., Ramanathan, T., Brinson, L. C., & Torkelson, J. M. (2008). Polymer-graphite nanocomposites: effective dispersion and major property enhancement via solid-state shear pulverization. *Macromolecules*, *41*(6), 1905-1908.

Zhang, C., & Zhu, Y. (2005). Synthesis of square Bi_2WO_6 nanoplates as high-activity visible-light-driven photocatalysts. *Chemistry of Materials*, *17*(13), 3537-3545.

Xu, C., Wei, X., Ren, Z., Wang, Y., Xu, G., Shen, G., & Han, G. (2009). Solvothermal preparation of Bi_2WO_6 nanocrystals with improved visible light photocatalytic activity. *Materials Letters*, *63*(26), 2194-2197.

Zhang, L., Wang, W., Chen, Z., Zhou, L., Xu, H., & Zhu, W. (2007). Fabrication of flower-like Bi_2WO_6 superstructures as high performance visible-light driven photocatalysts. *Journal of Materials Chemistry*, *17*(24), 2526-2532.

Shang, M., Wang, W., & Xu, H. (2008). New Bi_2WO_6 nanocages with high visible-light-driven photocatalytic activities prepared in refluxing EG. *Crystal Growth and Design*, *9*(2), 991-996.

Wang, P., Chen, D., Liu, J., & Tang, F. (2006). Synthesis and Characterization of Monodisperse TiO_2 Colloid Particles. *ACTA PHYSICOCHIMICA SINICA*, *22*(3), 365.

Matos, J., Laine, J., & Herrmann, J. M. (1998). Synergy effect in the photocatalytic degradation of phenol on a suspended mixture of titania and activated carbon. *Applied Catalysis B: Environmental*, *18*(3), 281-291.

Loddo, V., Marcì, G., Martín , C., Palmisano, L., Rives, V., & Sclafani, A. (1999). Preparation and characterisation of TiO_2 (anatase) supported on TiO_2 (rutile) catalysts employed for 4-nitrophenol photodegradation in aqueous medium and comparison with TiO_2 (anatase) supported on Al_2O_3. *Applied Catalysis B: Environmental*, *20*(1), 29-45.

Choi, W. Y., Nam, H. W., Kwak, N. H., Huh, W., Kim, Y. R., Kang, M. W., ... & Dubey, J. P. (1997). Foodborne outbreaks of human toxoplasmosis. *Journal of Infectious Diseases*, *175*(5), 1280-1282.

Iengo, P., Aprile, G., Di Serio, M., Gazzoli, D., & Santacesaria, E. (1999). Preparation and properties of new acid catalysts obtained by grafting alkoxides and derivatives on the most common supports. Part III–grafting titanium alkoxides and sulphate derivatives on silica. *Applied Catalysis A: General*, *178*(1), 97-109.

Pilkenton, S., Hwang, S. J., & Raftery, D. (1999). Ethanol photocatalysis on TiO_2-coated optical microfiber, supported monolayer, and powdered catalysts: An in situ NMR study. *The Journal of Physical Chemistry B,103*(50), 11152-11160.

Yamashita, H., Honda, M., Harada, M., Ichihashi, Y., Anpo, M., Hirao, T., ... & Iwamoto, N. (1998). Preparation of titanium oxide photocatalysts anchored on porous silica glass by a metal ion-implantation method and their photocatalytic reactivities for the degradation of 2-propanol diluted in water.*The Journal of Physical Chemistry B, 102*(52), 10707-10711.

Herrmann, J. M. (1999). Heterogeneous photocatalysis: fundamentals and applications to the removal of various types of aqueous pollutants. *Catalysis today*, *53*(1), 115-129.

Hughes, D. L., & Reamer, R. A. (1996). The effect of acid strength on the Mitsunobu esterification reaction: carboxyl vs hydroxyl reactivity. *The Journal of organic chemistry*, *61*(9), 2967-2971.

Ma, J. F., Yang, J., Li, S. L., Song, S. Y., Zhang, H. J., Wang, H. S., & Yang, K. Y. (2005). Two Coordination polymers of Ag (I) with 5-sulfosalicylic acid. *Crystal growth & design*, *5*(2), 807-812.

Sawunyama, P., Jiang, L., Fujishima, A., & Hashimoto, K. (1997). Photodecomposition of a Langmuir-Blodgett film of stearic acid on TiO_2 film observed by in situ atomic force microscopy and FT-IR. *The Journal of Physical Chemistry B, 101*(51), 11000-11003.

Kominami, H., Kumamoto, H., Kera, Y., & Ohtani, B. (2001). Immobilization of highly active titanium (IV) oxide particles: A novel strategy of preparation of transparent photocatalytic coatings. *Applied Catalysis B: Environmental*, *30*(3), 329-335.

Peill, N. J., & Hoffmann, M. R. (1996). Chemical and physical characterization of a TiO_2-coated fiber optic cable reactor. *Environmental science & technology*, *30*(9), 2806-2812.

Hofstadler, K., Bauer, R., Novalic, S., & Heisler, G. (1994). New reactor design for photocatalytic wastewater treatment with TiO_2 immobilized on fused-silica glass fibers: photomineralization of 4-chlorophenol. *Environmental science & technology*, *28*(4), 670-674.

Peill, N. J., & Hoffmann, M. R. (1996). Chemical and physical characterization of a TiO_2 coated fiber optic cable reactor. *Environmental science & technology*, *30*(9), 2806-2812.

Yang, Q. H., Fu, X. X., Wang, J. Z., Bai, S. L., & Sun, Y. H. (2000). Photocatalytic Degradation of Water-soluble Dyes over $LaxSrxFeO_3$. *Chinese Journal of Applied Chemistry*, *17*(6), 588-591.

Takeda, N., Iwata, N., Torimoto, T., & Yoneyama, H. (1998). Influence of carbon black as an adsorbent used in TiO_2 photocatalyst films on photodegradation behaviors of propyzamide. *Journal of catalysis*, *177*(2), 240-246.

Torimoto, T., Ito, S., Kuwabata, S., & Yoneyama, H. (1996). Effects of adsorbents used as supports for titanium dioxide loading on photocatalytic degradation of propyzamide. *Environmental science & technology*, *30*(4), 1275-1281.

Qing, W. F., Ping, R. S., Ping, L. X., Wei, G. A. O., Kun, X. B., & Yu, Z. M. (2000). Photocatalytic Degradation Properties Studies of A New Nanocrystalline TiO_2 coating Film. *Chemical Research In Chinese Universities*, *10*, 074.

Song, K. Y., Park, M. K., Kwon, Y. T., Lee, H. W., Chung, W. J., & Lee, W. I. (2001). Preparation of transparent particulate MoO_3/TiO_2 and WO_3/TiO_2 films and their photocatalytic properties. *Chemistry of materials*, *13*(7), 2349-2355.

Chapter 3-The Synthesis of Graphene Modified Bi_2WO_6 and its Visible Light-Induced Photocatalysts

3.1 Introduction

As environmental problems have become increasingly prominent in the news and real life, the use of visible light photocatalysts to purify of pollutants have been attracting the attention of scientists, politicians and lay people throughout the world (Braslavsky et al., 1996). Commonly encountered air and water pollutants include halides, pesticides, toxic gases and organic compounds (i.e. paraffin, polyethylene, toluene, phenol homologues such as methylene blue and rhodamine) (Kuhn et al., 2006). The study of new photocatalytic technology has great significance in the future of pollution control and remediation (Daneshvar et al., 2003).

Photocatalytic degradation of pollutants is a rapidly advancing field (Tryk et al., 2000). The main crux of the degradation process is the oxidization of these harmful substances into harmless basic molecules such as water and carbon dioxide (Malato et al., 2009). Currently, most researchers use semiconductor materials (such as TiO_2, $BiVO_4$, $InTaO_4$, Bi_2WO_6) as photocatalysts (Rajeshwar et al., 2008). Among them, Bi_2WO_6's narrowband system (Zhang et al., 2010) can take advantage of visible spectrum ranges of sunlight to power the photocatalytic reaction (Cui et al., 2010). Of the synthesis methods listed in Chapter 2, the hydrothermal method is considered optimal as it is pollution-free and does not require high reaction temperatures (Hidaka

et al., 1996). Its simple synthesis method for application provides a good reason for commercialization.

3.2 Experimental Methods

3.2.1 Synthesis of Precursor Bi_2WO_6

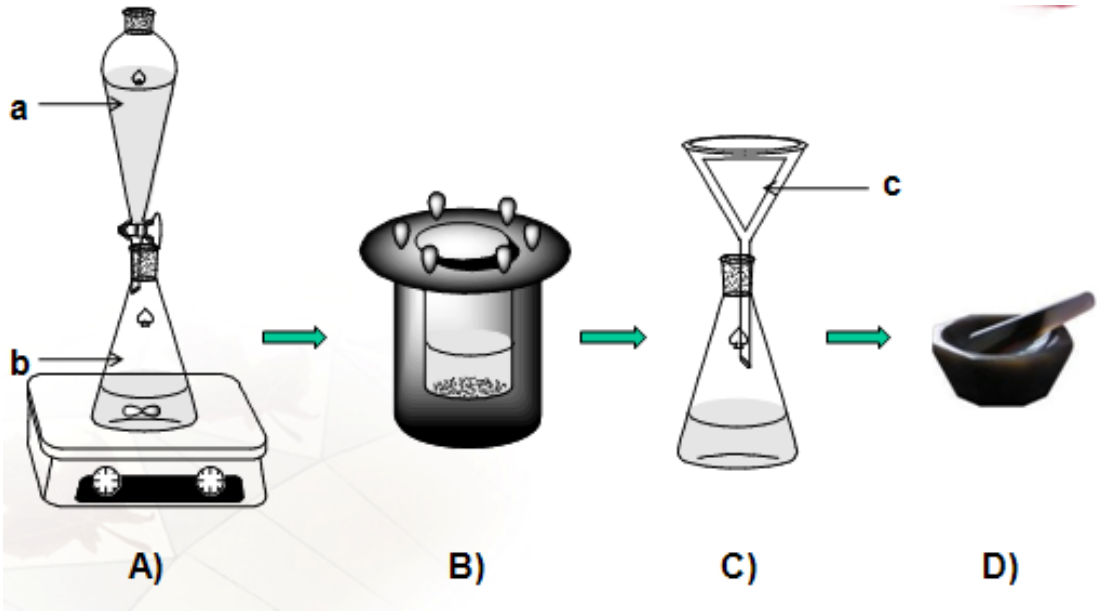

Figure 1- Procedure of Synthesis Precursor Bi_2WO_6

See Table 1 for source of reagents and equipments.

0.66 g $Na_2WO_4 \cdot 2H_2O$ was dissolved in 40 mL distilled deionized water. This mixture was designated “solution a”.

1.96 g $Bi(NO_3)_3 \cdot 5H_2O$ was dissolved in 80 mL glacial acetic acid and stirred for 10 min until completely dissolved. This mixture is designated “solution b”.

The white precipitate in Figure 1 is the precursor Bi_2WO_6. This product is designated “powder c”.

A) “Solution a” was added dropwise into “solution b” with stirring. The addition process took 30 min. Concentrated hydrochloric acid solution was used to adjust the resultant suspension to pH 1.

B) The suspension was transferred into a Teflon-lined stainless-steel autoclave. The autoclave was filled to 70% full (by volume). The autoclave was heated in an electric oven at 180 °C for 20 hours, then gradually cooled down to room temperature.

C) The resulting sample was firstly filtered by filter paper, washed twice with distilled deionized water and dried overnight.

D) The dry residue was ground for 5 min with a mortar and pestle to produce a white powder (Precursor Bi_2WO_6).

3.2.2 Graphene Modified Bi_2WO_6

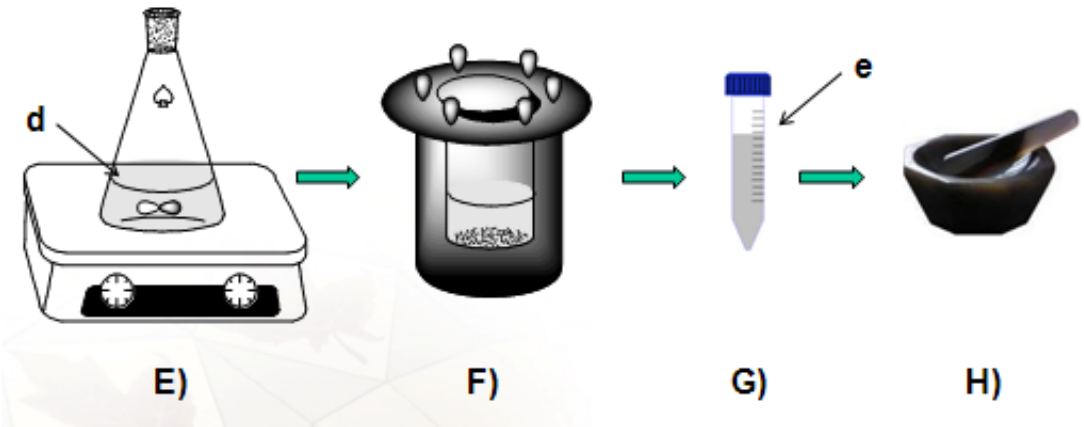

Figure 2- Procedure of Synthesis Graphene Modified Bi_2WO_6

1 g Bi_2WO_6 was dispersed into 70 mL of distilled deionized water and sonicated for 30 min to produce an even suspension of Bi_2WO_6. This mixture was designated “solution d”.

The gray precipitate is the GO-Bi_2WO_6. This product is designated “powder e”.

E) 1 mL GO dispersion solution (4mg/mL) was added into the suspension and the mixture magnetically stirred for two hours.

F) The mixture was transferred to a Teflon-lined stainless-steel autoclave (the autoclave was filled to 70% full by volume) and heated in an electric oven at 140 °C for 6 hours, then gradually cooled down to room temperature.

G) The resulting sample was centrifuged for 15 min, the supernatant was discarded and the solid precipitate was collected and dried overnight.

H) The dry residue was ground for 5 min with a mortar and pestle to produce a grey powder which is 0.4% (g/g) GO-Bi_2WO_6. The same procedure was repeated to obtain GO-BWO samples with different mass percentages of GO. For 0.8% (g/g) 2 mL GO dispersion solution was used. For 1.2% (g/g) 3 mL GO dispersion solution was used. For 1.6% (g/g) 4 mL GO dispersion solution was used.

3.2.3 Characterization

The crystal structures and the purity of the samples were characterized by X-ray diffraction (XRD) with a Cu-Kα radiation diffractometer recording with a 2θ scope ranging from 10-80º.

X-ray photoelectron spectra (XPS) data were collected on a Kratos Axis Ultra spectrometer with monochromatized Al K radiation at 14 kV and 140 W. The binding energies were referred to the C 1s hydrocarbon peak at 283 eV.

Scanning electron microscopy (SEM) was used to take images of the prepared Bi_2WO_6 samples employing an accelerating voltage of 5 kV or 20 kV.

Scanning transmission electron microscopy (STEM) was used to take images of the prepared GO-Bi_2WO_6 samples as graphene is too thin to be observed via SEM.

The UV-vis diffusion reflectance spectrum of the samples was analyzed using a UV-vis spectrophotometer (Thermo Evolution 300) equipped with an accessory for analyzing powder samples.

3.2.4 Batch Degradation Studies

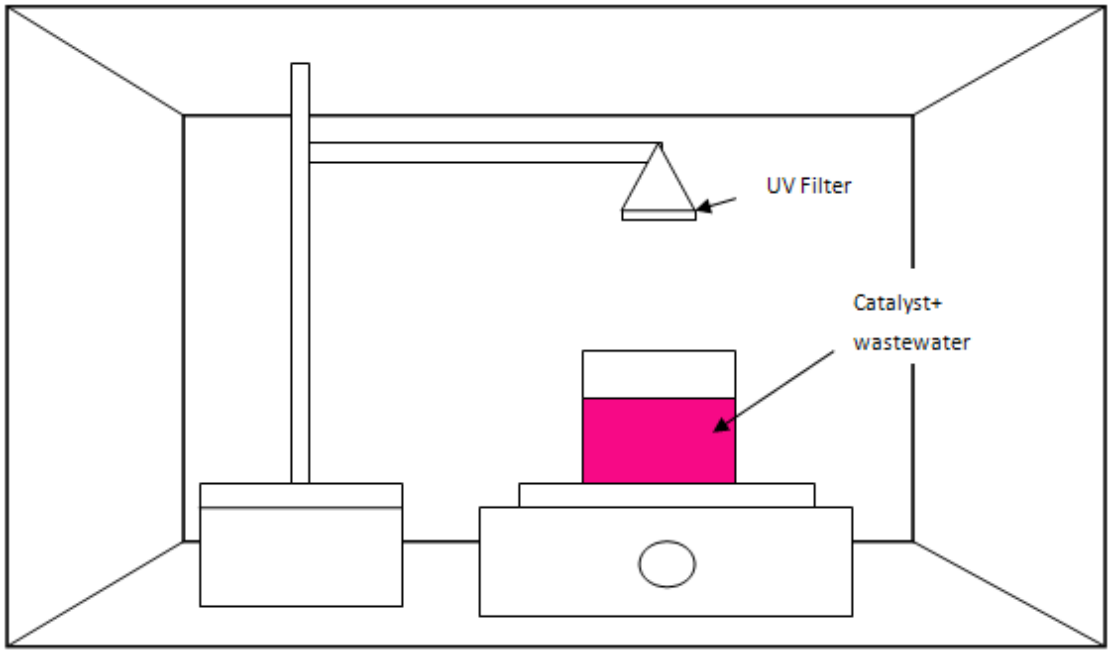

Figure 3- Schematic of Photocatalytic Degradation Experiments

The photocatalytic activity of each sample was evaluated by their ability to degrade the model pollutant (and fluorescent dye) Rhodamine B (Figure 4) dissolved in water. Procedures of activity tests were listed below.

a. A 300 Watt tungsten halide lamp was used to simulate sunlight, and a filter was used to cut off any radiation below 420 nm to ensure the photocatalysis was proceeding under visible light irradiation alone.
b. The temperature of the reaction vessel was controlled using a recirculating water jacket set to 20 ^{o}C ± 2 to avoid the effects of thermal catalytic reaction.
c. Given amounts of GO-Bi_2WO_6 photocatalysts were added to a 500 mL beaker containing 200 mL 10 ppm RhB aqueous solution.
d. The pH value of the mixture was adjusted using concentrated sodium hydroxide or hydrochloric acid.
e. Before illumination, the slurry was magnetically stirred in total darkness for 30 min to achieve adsorption/desorption equilibrium (Banihashemi et al., 2014).
f. 1 mL of the suspension was aliquoted into a centrifuge tube and centrifuged at 12000 rpm for 3 min. The absorbance of the liquid phase was determined using a Genysys UV-vis spectrophotometer. The above sampling and absorbance testing was done once every 10 minutes for the last 2 hours of the reaction duration (at each time point, the temperature of the bath was also recorded).

Dark control: procedure is the same as the main activity test with the exception that the reaction proceed in total darkness instead of light irradiation.

Light control: procedure is the same as the main activity test with the exception that the reaction proceed without photocatalyst to investigate the effect of dye photolysis.

Calibration curve: procedure was created in a separate experiment to determine the relationship between absorbance (λ_{max}= 552 nm) and concentration of RhB (Chang et al., 2012).

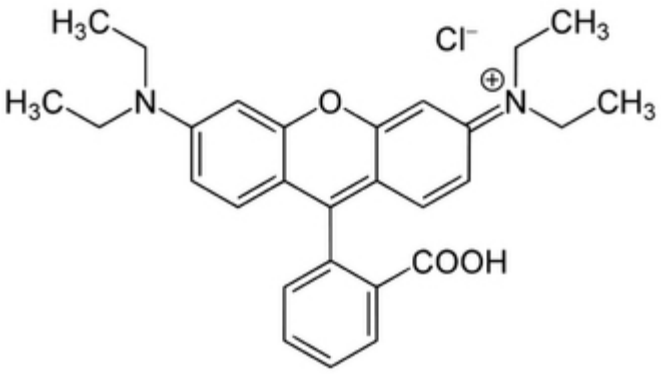

Figure 4 – Molecular Structure of RhB

Adapt from (Chang et al., 2012)

A UV-vis spectrophotometer was used to measure the retention concentrations of RhB solutions. By monitoring the change in absorbance of the residual dye solutions at RhB's maximum absorbance wavelength (λ= 552 nm), RhB concentration can be determined. The current dye absorption amount (q_t) was calculated from eq. 1 (Atulegwu Patrick et al., 2014).

$$q_t = \frac{V(C_0 - C_t)}{W} \quad (1)$$

At equilibrium, $q_t = q_e$ $C_t = C_e$; the amount of adsorbed dye, q_e was calculated from eq. 2 (Atulegwu Patrick et al., 2014).

$$q_e = \frac{V(C_0 - C_e)}{W} \quad (2)$$

Where C_0 is the initial concentration of RhB (mg/L), C_t is the current concentration at time t (mg/L), C_e is the equilibrium concentrations of dye solution (mg/L), V is the

volume of the solution (L), and W is the mass of adsorbent (g) (Atulegwu Patrick et al., 2014; Elmorsi et al., 2014).

The photocatalytic degradation efficiency was calculated by the following equation:

$$\text{Degradation efficiency}(\%) = \frac{C_0 - C_t}{C_0} * 100\% \quad (3)$$

Where C_0 is the initial concentration of RhB (mg/L). C_t is the concentration (mg/L) at time t (min) after the start of the reaction (Herrmann et al., 1999).

Table 1- Experimental Reagents and Relevant Information

Chemical Name	Grade	Manufacturer	Lot Number
Sodium Tungstate Dihydrate	BioUltra grade, 99.5%	Sigma	BCBD7104V
Bismuth Nitrate Pentahydrate	ACS reagent grade, 98%	Sigma-Aldrich	MKBF1293V
Acetic Acid	ACS pure	Fisherbrand	512334
Graphene Oxide Solution	4mg/mL	Aldrich	MKBP2325V
Rhodamine B	dye content, 95%	Fisher Chemical	094958
Hydrochloride Acid	0.5 mol/L	Fisherbrand	213094
Sodium Hydroxide	0.5 mol/L	Fisherbrand	863423

3.3 Results and Discussion

The author would like to thank the Center for Catalysis Research and Innovation and the Department of Earth Sciences at the University of Ottawa for help with sample characterization.

3.3.1 XRD Analysis

When high-speed electrons are bombarding atoms, atomic core electrons will transit and produce a continuous X-ray beam and a characterized X-ray beam. Atoms in a crystal structure may exhibit X-ray interference effects, resulting in a maximum intensity beam. Diffraction strengthening effect will occur according to the Bragg diffraction formula: $2d\sin\theta=\lambda$. By using known wavelengths of X-ray to measure the angle θ, the interplanar spacing (d) can be determined, which is used for analysis of crystal structure. Inversely, if d is known, we can use it to determine angle θ, and calculate the X-ray wavelength of the crystal. The elements contained in the sample can be found in existing data (Tang et al., 2004). XRD peak positions (diffraction angle) can determine the crystal plane spacing of this group, which Bi_2WO_6 with the theoretical calculations of the relative ratio of the cluster plane, which determine whether the Bi_2WO_6 crystal or crystal surface is complete or not.

Bi_2WO_6 crystallinity is a significant factor that influences photocatalytic activity. Defects in the crystal structure can cause recombination of photo-generated electrons

and holes, which results in a dramatic decline of catalytic activity (Ying et al., 2011). The higher the degree of crystallinity of Bi_2WO_6, the fewer amorphous defects there are, reducing the probability of recombination. Therefore, preparing Bi_2WO_6 by the hydrothermal method while retaining high-crystallinity is an issue that must be solved. Since the precursor is amorphous, Bi_2WO_6 will form crystalline phases when prepared using the hydrothermal method. Heat and time are needed to provide enough energy to overcome the energy barrier separating disordered crystal types from ordered crystal types during the transition process (Chen et al., 2013). Currently, 120 ℃ is recognized as the temperature where the crystallization begins. The optimal crystallization temperature is 180 ℃ as previous studied (Gao et al., 2011).

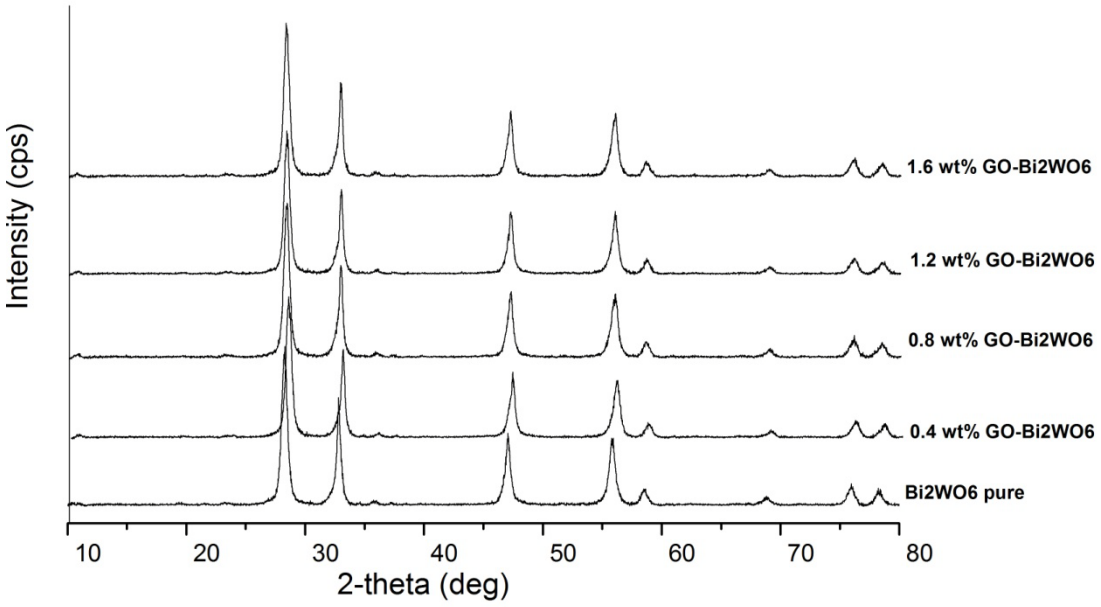

Figure 5- XRD Patterns of Hydrothermally Synthesized Bi_2WO_6 Before and After Composite with Various Contents (0.4 wt%-1.6 wt%) of Graphene Oxide

To prove that the hydrothermal product is an ordered Bi_2WO_6 crystal, pure Bi_2WO_6 and GO-Bi_2WO_6 were characterized by XRD (Figure 5). By comparing the results of our samples to that of the pure Bi_2WO_6 XRD pattern, we can roughly estimate the degree of crystallization of our Bi_2WO_6 samples. All the diffraction peaks in the XRD patterns of the samples were indexed to the standard data for Bi_2WO_6 (DB Card No.: 01-075-5628). The shape of crystal peaks were clean, with no amorphous characteristic peaks (Chen et al., 2013). This indicates that the synthesized Bi_2WO_6 had a good degree of crystallinity and was expected to have good catalytic activity. Modification of this material by GO with different contents (0.4 wt%-1.6 wt%) did not produce any changes in the peak positions or shapes, compared to the pattern of the pure Bi_2WO_6 (Gao et al., 2011). The main reason that GO has such a small impact on Bi_2WO_6 is that the crystallinity of GO is not as good as most crystals (Ying et al., 2011; Chen et al., 2013). XRD peaks belonging to amorphous-type crystals have low intensities, and such a small amount (0.4 wt%-1.6 wt%) of modification is not sufficient to change the XRD diffraction peaks positions or shapes of Bi_2WO_6. From the XRD data, it was concluded that graphene modification and the hydrothermal synthesis method of Bi_2WO_6 did not affect the crystal structure of the Bi_2WO_6 photocatalyst.

3.3.2 XPS Analysis

In X-ray Photoelectron Spectroscopy (XPS), samples are radiated by X-ray so that the inner electrons or valence electrons of atoms are stimulated and emitted. The electrons stimulated by photons are called photoelectrons (Xiao et al., 2008). Photoelectron kinetic energy is plotted on a graph using binding energy (eV) as the x-axis and the relative intensity (pulse/s) as the y-axis. From this photoelectron spectrum graph, we can derive the photoelectron spectrum (Drelinkiewicz et al. 2009). We can determine what are the element constituents of the sample molecules, their chemical valence states and so on.

XPS was used to investigate the composition of surface element and the chemical state of the elements in the GO-Bi_2WO_6 photocatalyst (Figures 6-9), XPS surveys were obtained by scanning the C 1s, O 1s, Bi 4f and W 4f levels (Gao et al., 2011; Zhou et al., 2012).

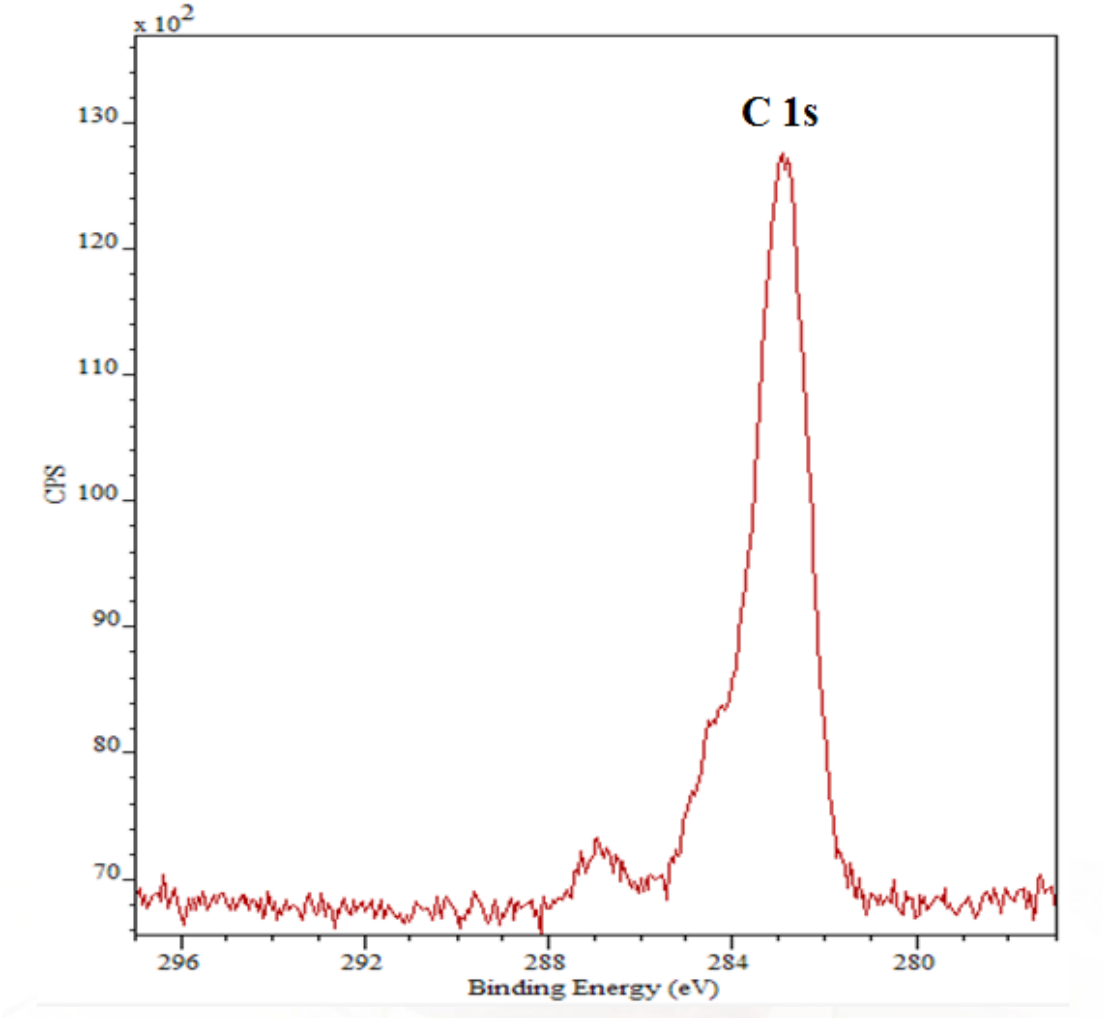

Figure 6- XPS Spectrum of Carbon in GO-Bi_2WO_6 Composite Sample

There are no carbon atoms in Bi_2WO_6, indicating that the carbon is from graphene. Carbon atoms are also used for calibration.

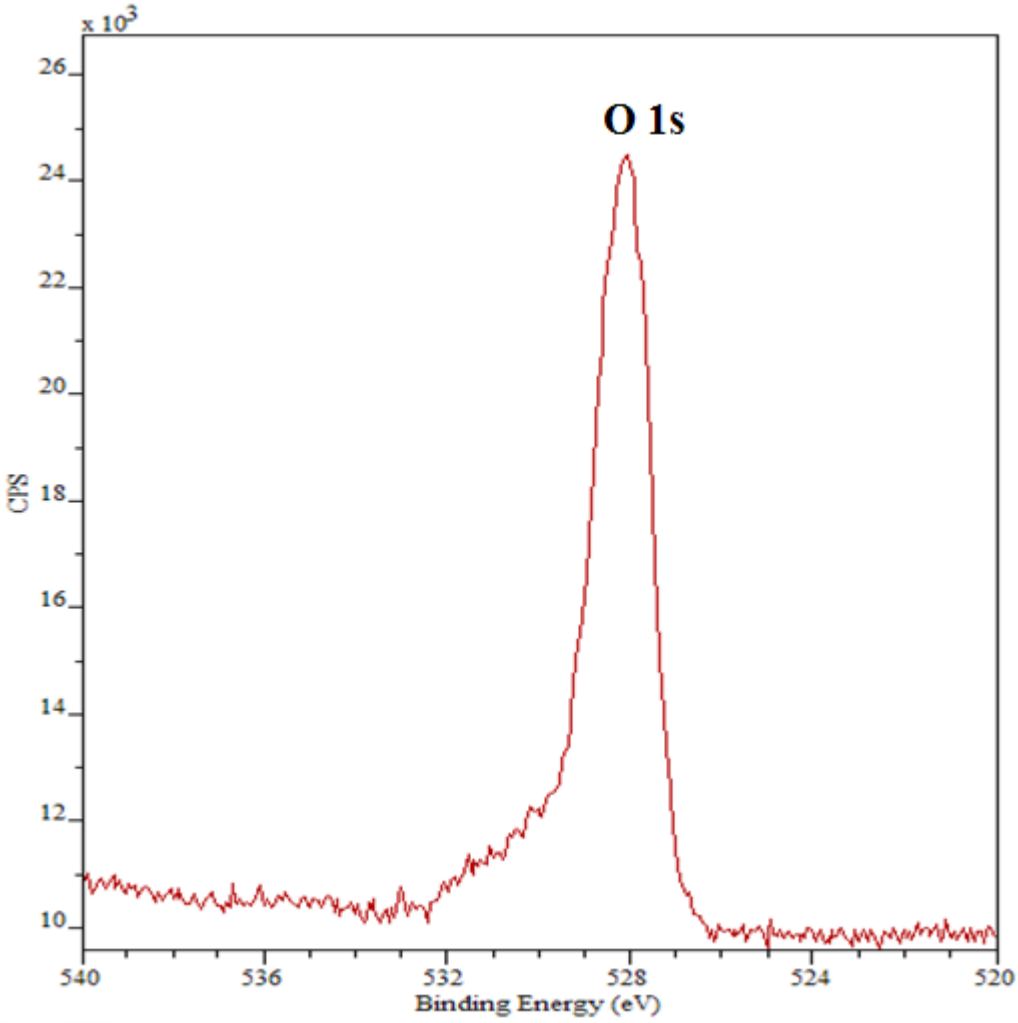

Figure 7- XPS Spectrum of Oxygen in GO-Bi_2WO_6 Composite Sample

In XPS spectrum for O 1s level, the peak position is at 528 eV, demonstrating that the oxygen species are characteristic of lattice oxygen in Bi_2WO_6 (Xiao et al., 2008; Zhang et al., 2013).

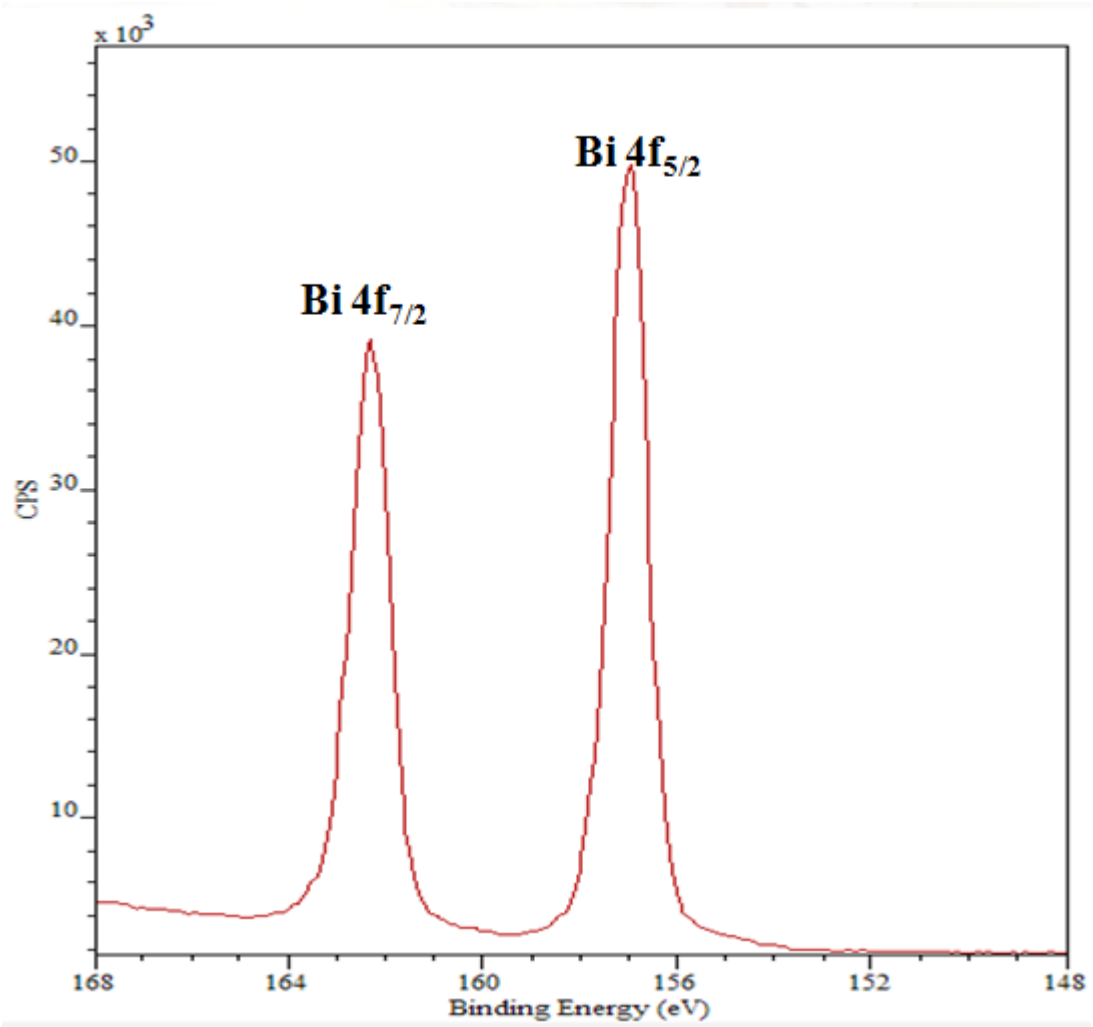

Figure 8- XPS Spectrum of Bismuth in GO-Bi_2WO_6 Composite Sample

In XPS spectrum for Bi $4f_{7/2}$ and $4f_{5/2}$ levels, the binding energies were observed at 163.1 eV and 157.6 eV, respectively (Zhang et al., 2013), revealing a trivalent oxidation state for bismuth. (Bi^{3+}) as it occurs in Bi_2WO_6 (Zhang et al., 2013).

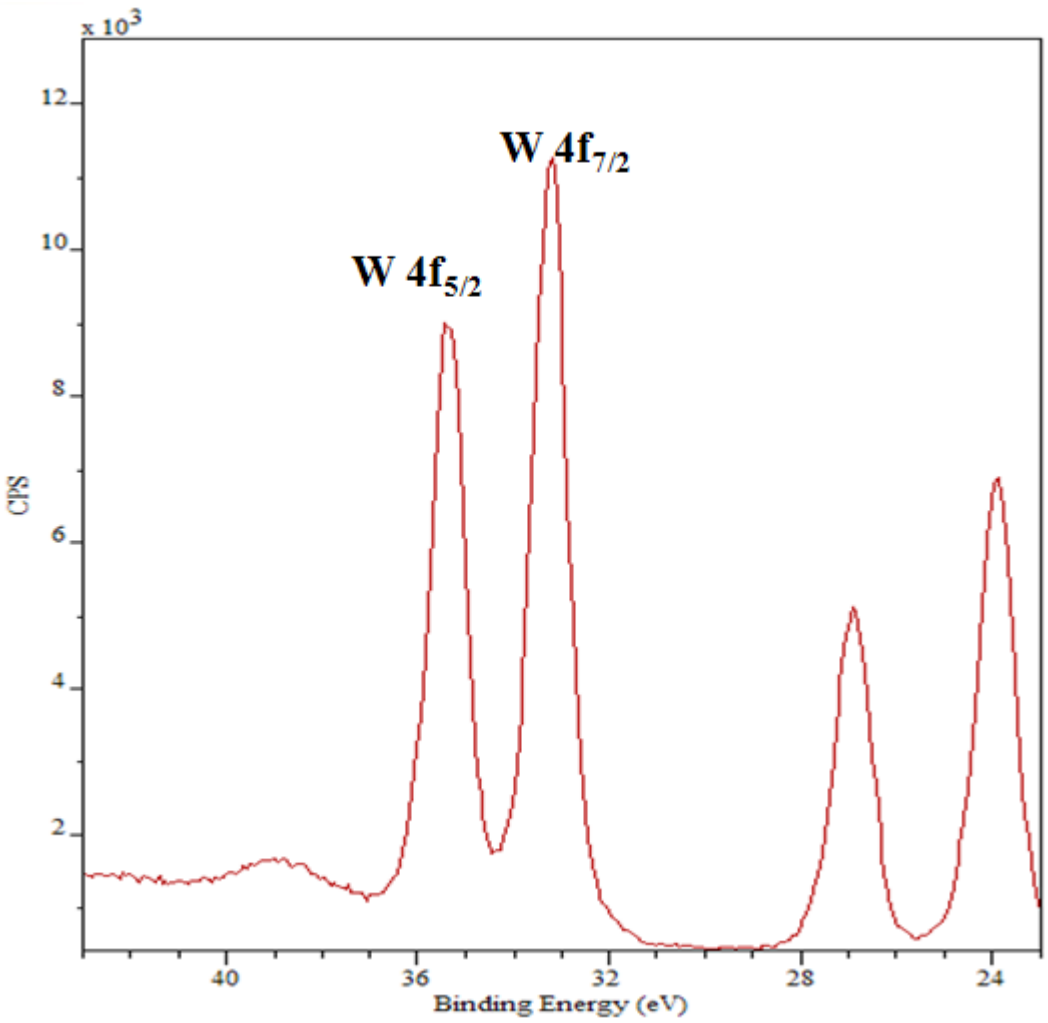

Figure 9- XPS Spectrum of Tungsten in GO-Bi_2WO_6 Composite Sample

In XPS spectrum for W $4f_{5/2}$ and $4f_{7/2}$ levels, the binding energies were observed at 35.8 eV and 33.5 eV, respectively (Ren et al. 2009), indicating a hexavalent oxidation state of tungsten (W^{6+}) as it occurs in Bi_2WO_6.

All the results showed that the samples produced were the expected Bi_2WO_6 photocatalyst.

3.3.3 SEM Analysis

Scanning Electron Microscopy (SEM) was used to observe the macroscopic morphology of Bi_2WO_6. Due to the low resolution of SEM, we can only visualize the surface of Bi_2WO_6 and macroscopic morphology changes (Zhou et al., 2012; Xie et al., 2014).

Different two-dimensional and three-dimensional forms of Bi_2WO_6 can be obtained by adjusting the pH, reaction time, and raw content of the reaction solution (e.g. by adding a surfactant) (Zhou et al., 2012; Zhang et al., 2013). The photocatalytic activities of these different forms of Bi_2WO_6 are different. Bi_2WO_6 morphology control is very important to maintain the catalytic efficiency. In order to study the macroscopic morphology of Bi_2WO_6 after compositing with graphene, SEM tests were done both before and after composing with GO. The comparison chart is shown in Figure 10-13 as follows.

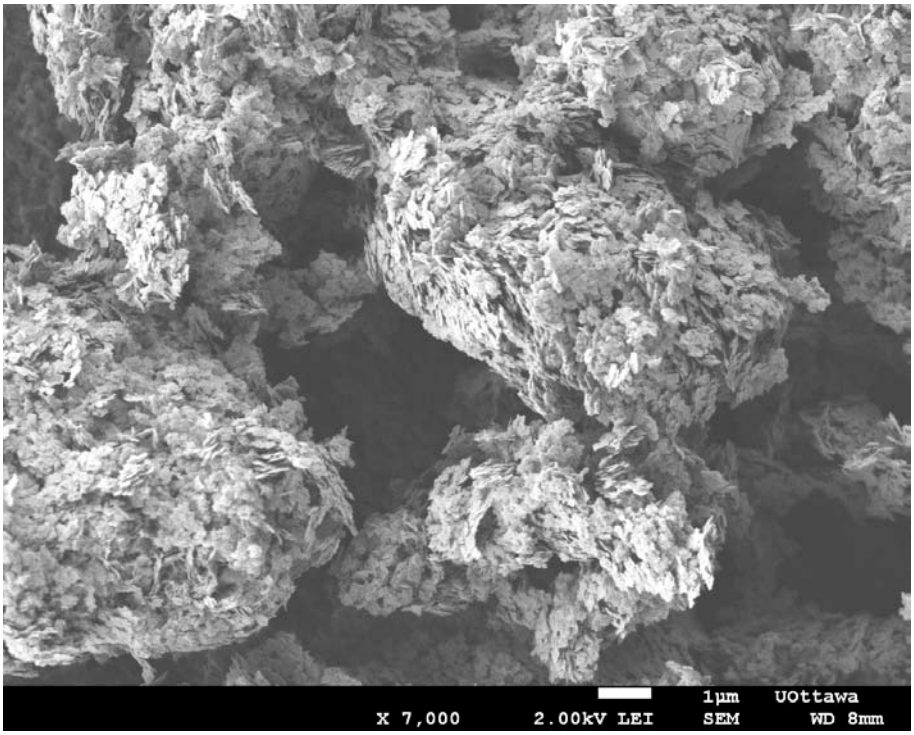

Figure 10- SEM Images of Hydrothermally Synthesized Bi_2WO_6 in a Three-Dimensional Shape

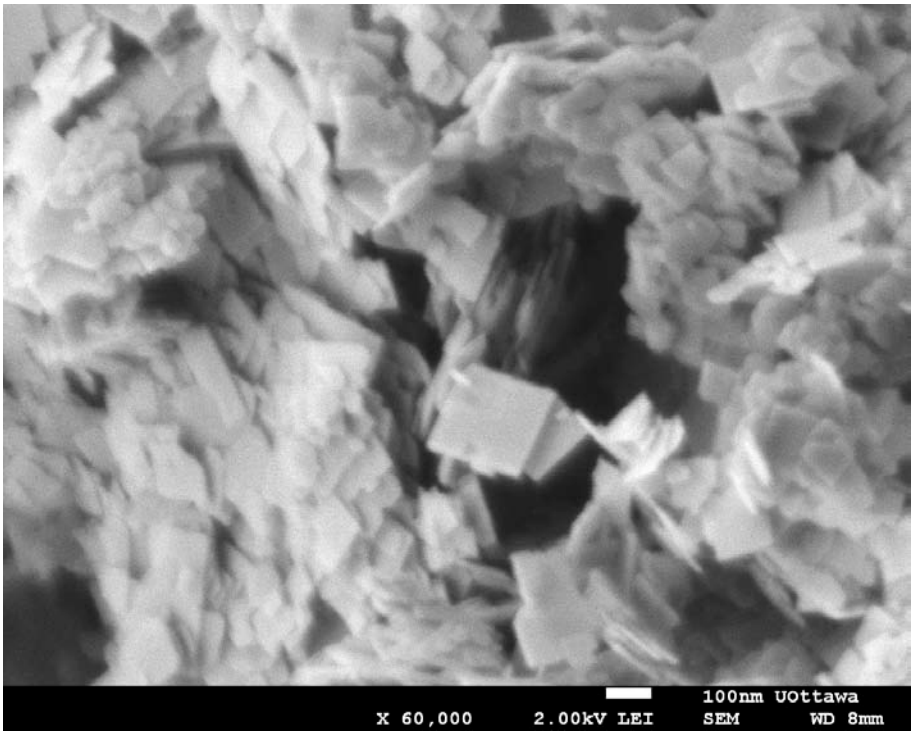

Figure 11- SEM Images of Hydrothermally Synthesized Bi_2WO_6 Plates

From Figures 10-11, the obtained pure compound Bi_2WO_6 was observed in a three-dimensional shape. The cluster was made up of many small pieces stacked.

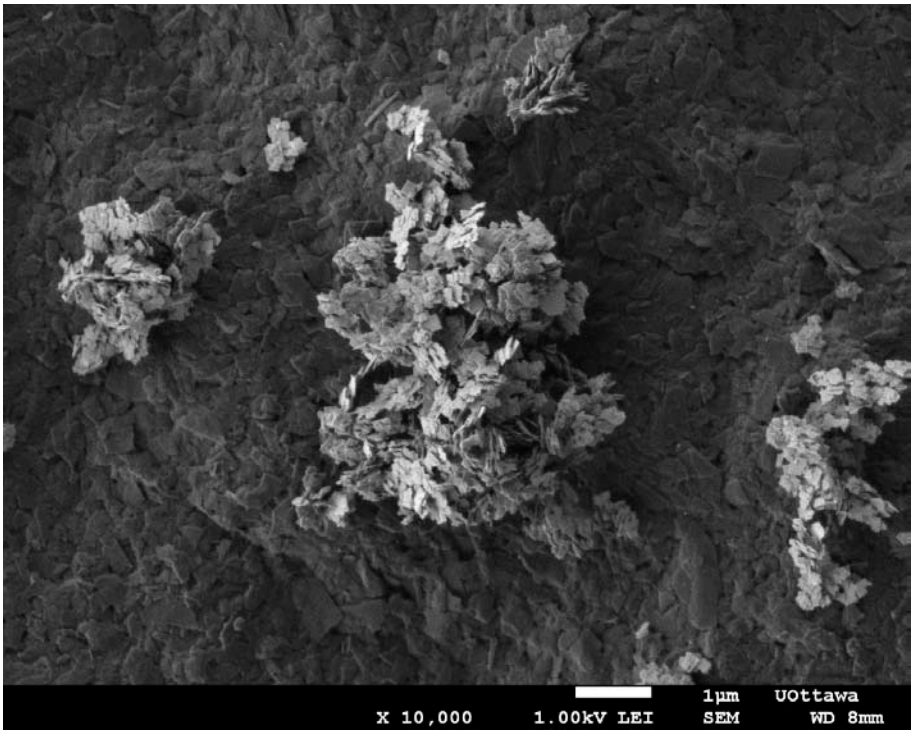

Figure 12- SEM Images of Composite GO-Bi_2WO_6 in a Three-Dimensional Shape

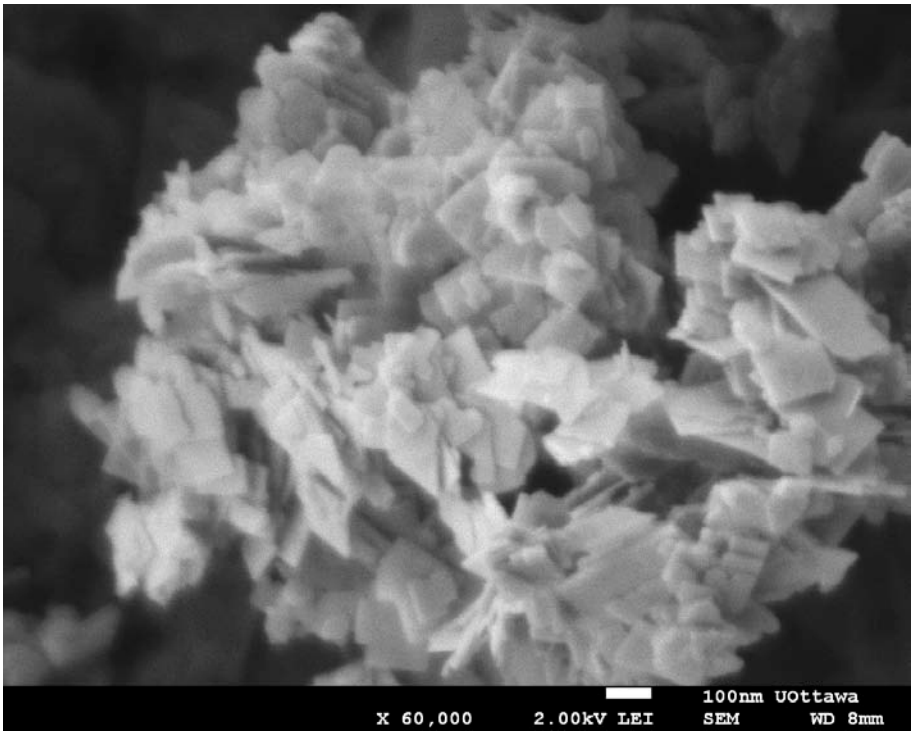

Figure 13- SEM Images of Composite GO-Bi_2WO_6 Plates

Bi_2WO_6 macroscopic morphology exhibited no major changes after GO modification from SEM micrographs. The sheet structures were the same. The presence of graphene cannot be seen in Figures 12-13 because graphene sheets are so thin, and the amount present was too low to be observed by such a low-resolution SEM. Figures 12-13 confirmed that after Bi_2WO_6 was modified by GO, its morphology only changed slightly (Low et al., 2014). So morphological changes should have minimal effects on the photocatalytic activity of the catalyst. Further confirming the graphene could improve the photocatalytic activity (Sun et al., 2013).

3.3.4 STEM Analysis

As the presence of graphene cannot be verified using macro-morphology SEM images, graphene oxide composite Bi_2WO_6 can be more effectively characterized using Scanning Transmission Electron Microscopy (STEM), which has a higher-resolution than SEM (Low et al., 2014). STEM is commonly used to study the crystallization of nanomaterials, observing nano-particle morphology, evaluating nanoparticle dispersion and measuring nano-particle diameter. It is one of the common characterization techniques for nanocomposites microstructures (Sun et al., 2013).

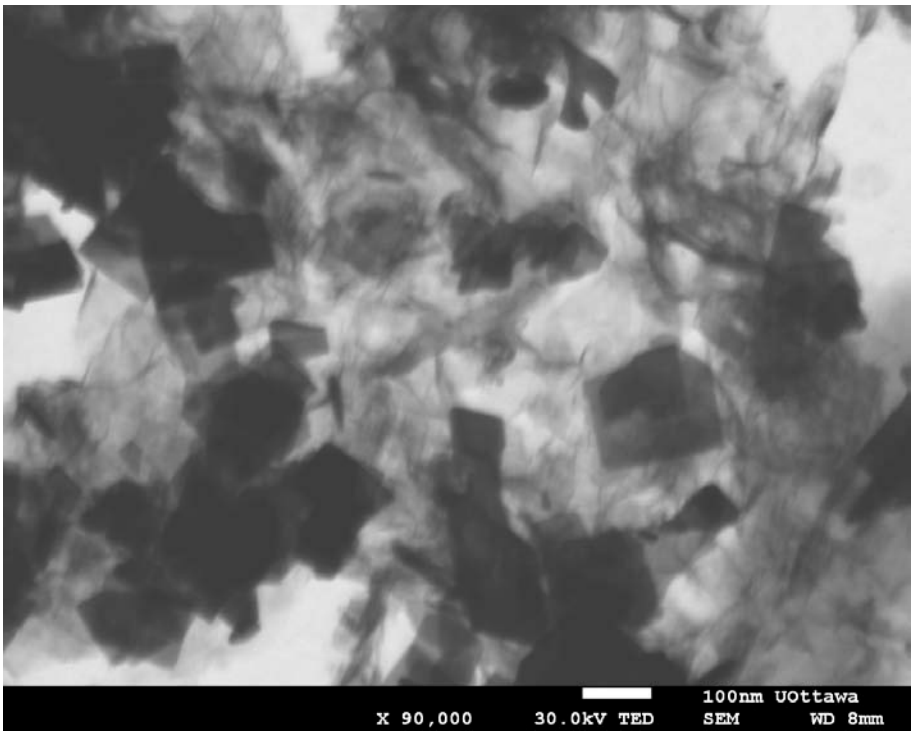

Figure 14- STEM Images of Composite GO-Bi_2WO_6 Overall View

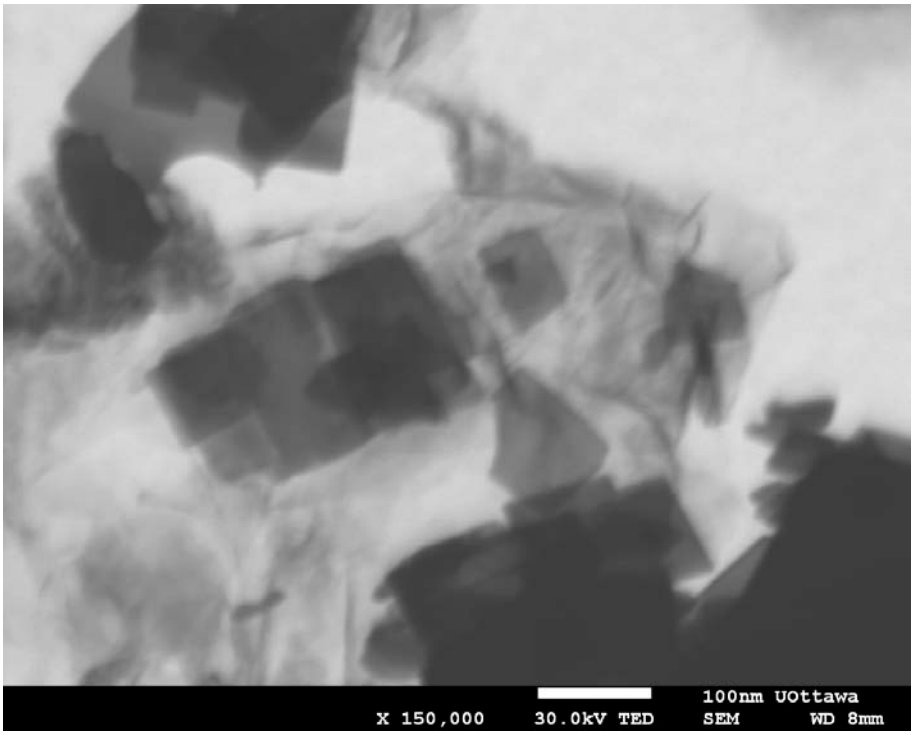

Figure 15- STEM Images of GO in Conjunction with Bi_2WO_6

As seen in the above images, Bi_2WO_6 particles are too thick to allow transmission electrons to penetrate completely, these blocked areas show up black on the images. The black squares in Figure 14 are Bi_2WO_6. The translucent nets in the same figure are GO (Sun et al., 2013). In Figure 15, GO can be seen close in conjunction with Bi_2WO_6. GO adheres to the edge of Bi_2WO_6. From the STEM image, it can be concluded that GO and Bi_2WO_6 indeed form a complex structure.

3.4 Conclusion

Based on these experiments, it can be inferred that GO-Bi_2WO_6 was effectively synthesized through a template-free hydrothermal method. The synthesized GO-Bi_2WO_6 samples were characterized by using XRD, SEM and STEM in order to gain insight into the crystallinity, morphology and structure of the photocatalyst. By XRD, SEM and STEM observation, it was found that the participation of GO did not affect the crystal lattice of Bi_2WO_6. GO and Bi_2WO_6 indeed formed a complex catalyst.

3.5 References

Braslavsky, S. E., Houk, K. N., & Verhoeven, J. W. (1996). Glossary of terms used in photochemistry. *International Union of Pure and Applied Chemistry*.

Hidaka, H., Suzuki, Y., Nohara, K., Horikoshi, S., Hisamatsu, Y., Pelizzetti, E., & Serpone, N. (1996). Photocatalyzed degradation of polymers in aqueous semiconductor suspensions. I. Photooxidation of solid particles of polyvinylchloride. *Journal of Polymer Science Part A: Polymer Chemistry*, *34*(7), 1311-1316.

Daneshvar, N., Salari, D., & Khataee, A. R. (2003). Photocatalytic degradation of azo dye acid red 14 in water: investigation of the effect of operational parameters. *Journal of Photochemistry and Photobiology A: Chemistry*, *157*(1), 111-116.

Kuhn, H. J., Braslavsky, S. E., Schmidt, R., Terazima, M., Hirota, N., Mandelis, A., ... & Houk, K. N. (1984). Glossary of terms used in photochemistry, (IUPAC Recommendations 2006). *Pure Appl. Chem*, *56*(9), 1153-1165.

Tryk, D. A., Fujishima, A., & Honda, K. (2000). Recent topics in photoelectrochemistry: achievements and future prospects. *Electrochimica acta*, *45*(15), 2363-2376.

Malato, S., Fernández-Ibáñez, P., Maldonado, M. I., Blanco, J., & Gernjak, W. (2009). Decontamination and disinfection of water by solar photocatalysis: recent overview and trends. *Catalysis Today*, *147*(1), 1-59.

Rajeshwar, K., Osugi, M. E., Chanmanee, W., Chenthamarakshan, C. R., Zanoni, M. V. B., Kajitvichyanukul, P., & Krishnan-Ayer, R. (2008). Heterogeneous

photocatalytic treatment of organic dyes in air and aqueous media. *Journal of Photochemistry and Photobiology C: Photochemistry Reviews*, *9*(4), 171-192.

Cui, Z., Zeng, D., Tang, T., Liu, J., & Xie, C. (2010). Processing–structure–property relationships of Bi_2WO_6 nanostructures as visible-light-driven photocatalyst. *Journal of hazardous materials*, *183*(1), 211-217.

Zhang, Z., Wang, W., Shang, M., & Yin, W. (2010). Low-temperature combustion synthesis of Bi_2WO_6 nanoparticles as a visible-light-driven photocatalyst. *Journal of hazardous materials*, *177*(1), 1013-1018.

Banihashemi, B., & Droste, R. L. (2014). Sorption–desorption and biosorption of bisphenol A, triclosan, and 17α-ethinylestradiol to sewage sludge. *Science of The Total Environment*.

Chang, X., Gondal, M. A., Al-Saadi, A. A., Ali, M. A., Shen, H., Zhou, Q., ... & Ji, G. (2012). Photodegradation of Rhodamine B over unexcited semiconductor compounds of BiOCl and BiOBr. *Journal of colloid and interface science*, *377*(1), 291-298.

Atulegwu Patrick, U., Cosmas Chinedu, U., & Darlington, A. (2014). Analysis of Thermodynamics, Kinetics and Equilibrium Isotherm on Fe^{3+}/Fe^{2+} Adsorption onto Palm Kernel Shell Activated Carbon (PKSAC): *A Low-cost Adsorbent*. *American Chemical Science Journal, 4(3).*

Herrmann, J. M. (1999). Heterogeneous photocatalysis: fundamentals and applications to the removal of various types of aqueous pollutants. *Catalysis today*, *53*(1), 115-129.

Elmorsi, T. M. (2011). Equilibrium Isotherms and Kinetic Studies of Removal of Methylene Blue Dye by Adsorption onto Miswak Leaves as a Natural Adsorbent. *Journal of Environmental Protection*, *2*(6).

Tang, J., Zou, Z., & Ye, J. (2004). Photocatalytic decomposition of organic contaminants by Bi_2WO_6 under visible light irradiation. *Catalysis Letters*,*92*(1-2), 53-56.

Ying, H., Wang, Z. Y., Guo, Z. D., Shi, Z. J., & Yang, S. F. (2011). Reduced graphene oxide-modified Bi_2WO_6 as an improved photocatalyst under visible light. *Acta Physico-Chimica Sinica*, *27*(6), 1482-1486.

Chen, J., Shi, J., Wang, X., Cui, H., & Fu, M. (2013). Recent progress in the preparation and application of semiconductor/graphene composite photocatalysts. *Chinese Journal of Catalysis*, *34*(4), 621-640.

Xiao, Q., Zhang, J., Xiao, C., & Tan, X. (2008). Photocatalytic degradation of methylene blue over Co_3O_4/Bi_2WO_6 composite under visible light irradiation. *Catalysis Communications*, *9*(6), 1247-1253.

Drelinkiewicz, A., Sobczak, J. W., Sobczak, E., Krawczyk, M., Zięba, A., & Waksmundzka-Góra, A. (2009). Physicochemical and catalytic properties of Pt–poly (4-vinylpyridine) composites. *Materials Chemistry and Physics*,*114*(2), 763-773.

Gao, E., Wang, W., Shang, M., & Xu, J. (2011). Synthesis and enhanced photocatalytic performance of graphene-Bi_2WO_6 composite. *Physical Chemistry Chemical Physics*, *13*(7), 2887-2893.

Zhou, F., & Zhu, Y. (2012). Significant photocatalytic enhancement in methylene blue degradation of Bi_2WO_6 photocatalysts via graphene hybridization. *Journal of Advanced Ceramics*, *1*(1), 72-78.

Zhang, J., Huang, Z. H., Xu, Y., & Kang, F. (2013). Hydrothermal Synthesis of Graphene/Bi2WO6 Composite with High Adsorptivity and Photoactivity for Azo Dyes. *Journal of the American Ceramic Society*, *96*(5), 1562-1569.

Ren, J., Wang, W., Sun, S., Zhang, L., & Chang, J. (2009). Enhanced photocatalytic activity of Bi_2WO_6 loaded with Ag nanoparticles under visible light irradiation. *Applied Catalysis B: Environmental*, *92*(1), 50-55.

Low, J., Yu, J., Li, Q., & Cheng, B. (2014). Enhanced visible-light photocatalytic activity of plasmatic Ag and graphene co-modified Bi_2WO_6 nanosheets. *Physical Chemistry Chemical Physics*, *16*(3), 1111-1120.

Xie, X. D., Chen, C. S., Cao, S. Y., Liu, T. G., Huang, M. X., Chen, W. W., & Xiao, Y. (2014). Graphene Supported Small-sized ZnO Nanoparticles and Their Photocatalytic Property. *Integrated Ferroelectrics*, *153*(1), 177-183.

Sun, S., Wang, W., & Zhang, L. (2013). Bi_2WO_6 Quantum Dots Decorated Reduced Graphene Oxide: Improved Charge Separation and Enhanced Photoconversion Efficiency. *The Journal of Physical Chemistry C*, *117*(18), 9113-9120.

Chapter 4-Enhancement of Photocatalytic Performance

4.1 Introduction

This chapter will discuss the catalytic properties of GO- Bi_2WO_6 as well as the factors influencing its activity. Also, this chapter discusses the optimal ratio at which GO should be incorporated into Bi_2WO_6. Degradation rate constant and removal efficiency were analyzed by proceeding dynamic analysis (Xiang et al., 2012). Finally, this chapter discusses the optimal reaction conditions (dosage of catalyst, initial pH value of the solution and temperature) that yields the best catalytic activity (Zhang et al., 2013).

4.2 Calibration Curve

The calibration curve was determined by correlating absorbance (λ=552 nm) (Gao et al., 2011) and concentration of Rhodamine B (RhB) solution (Figure 1).

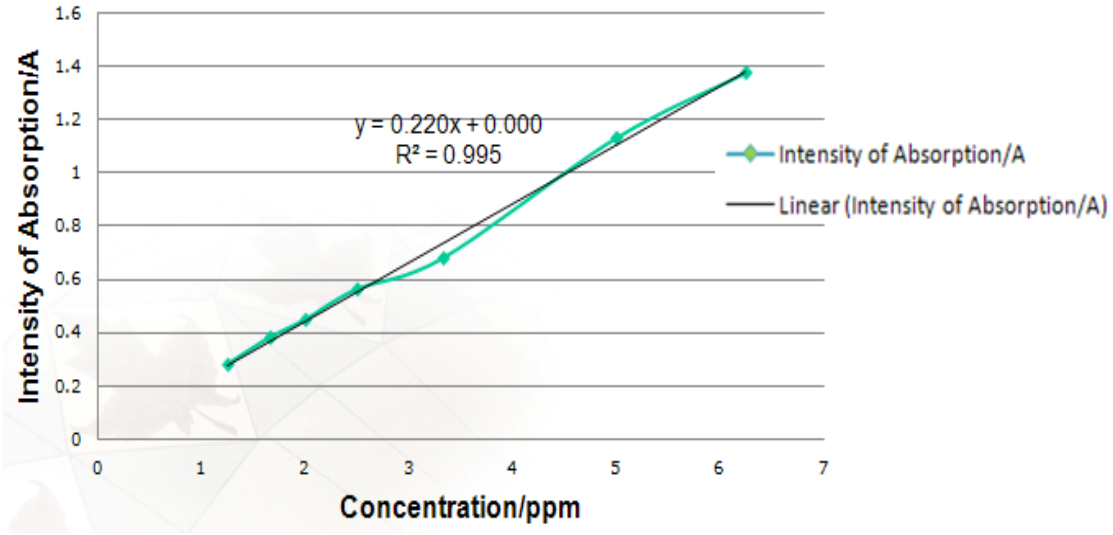

Figure 1- The Calibration Curve of Rhodamine B

RhB was the chosen model pollutant for these experiments. To prepare RhB solutions, stock RhB solutions (100 mg/L) were prepared by dissolving 0.1 g RhB powder into 1000 ml of distilled deionized water. The stock solution was further diluted to produce required concentrations for the experiments (1.25 ppm, 1.66 ppm, 2 ppm, 2.5 ppm, 3.3 ppm, 5 ppm and 6.25 ppm in this study). The upper bound of the absorbance curve was set at 1.5 Å (absorbance values are not reliable beyond 1.5 Å). The relationship between concentration and absorption is linear, and the equation of Abs-con. is y=0.220x.

4.3 Catalytic Performance

4.3.1 Contrast of Activities for Two Catalysts and Control Conditions

In order to evaluate the photocatalytic activity of composite catalysts, the ultraviolet absorption test was used to determine the decrease in Rhodamine B concentration in real time (the test was done once every 10 minutes for 90 minutes). Thus, we compared the photocatalytic reactions of Bi_2WO_6 before and after compositing with GO. Additionally, two control experiments were done. The first was to determine the rate degradation of RhB under illumination alone without catalyst. The second was to determine the catalyst's rate of RhB degradation in the absence of all light. To better understand the rate of photocatalytic reaction, RhB remaining concentration ratio ($C:C_0$) will be plotted as y-axis. The degradation time will be plotted as the x-axis. For comparative purpose, all experimental conditions were kept the same except for the catalysts and light.

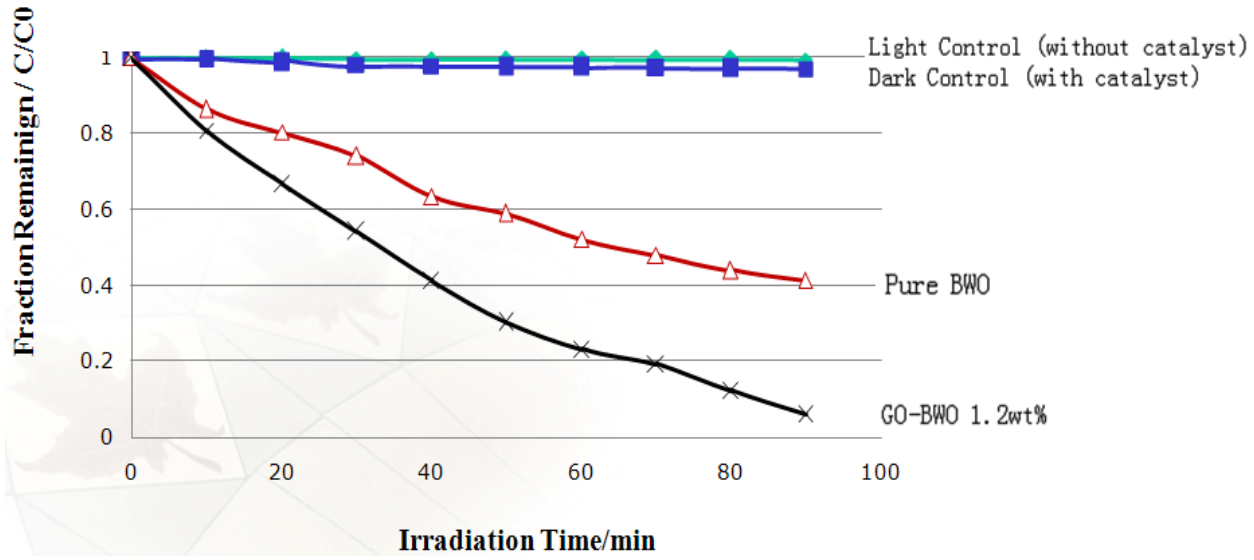

Figure 4- Degradation Curves of Rhodamine B (a) Light Control (No Catalyst) (b) Dark Control (No Light) (c) Pure Bi_2WO_6 (d) 1.2 wt% GO-Bi_2WO_6

Photocatalytic activity of pure BWO and GO-BWO was evaluated by degradation of RhB under visible light irradiation (Figure 2). Under visible light irradiation, catalytic activity was greatly improved by GO modification. Modified GO-Bi_2WO_6's photocatalytic efficiency reached as high as 95% with 1.2 wt% GO.

In the light control, the RhB solution was irradiated without the catalyst present. No obvious RhB degradation was observed. This suggests that Rhodamine B cannot degrade spontaneously without catalyst. The dye was stable under visible light irradiation, which shows that the dye degradation is due to the activity of the catalyst.

In dark control, the catalyst was added to the RhB solution but the solution was not irradiated. The concentration ratio declined slightly after 90 min, but declined magnitude was faster than that of the light control. The reason is that although catalyst is not active in darkness, but it can physically absorb a small amount of RhB and

remove it from the solution. It indicates that the absorption of RhB has a negligible impact on reaction after the adsorption-desorption equilibrium.

4.3.2 Contrast of Activities for Bi_2WO_6 Incorporated into Different Content of GO

The effect changing the percentage of GO incorporated into Bi_2WO_6 on RhB degradation was studied (Figure 3). The initial concentration of RhB was kept at 10 ppm, and the content of GO varied from 0.4 wt% to 1.6 wt%.

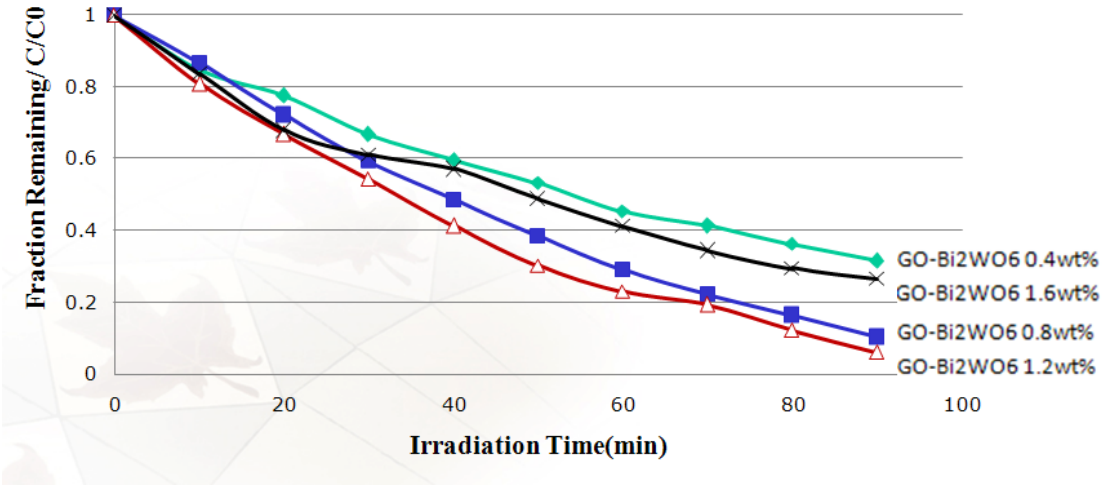

Figure 3- Fraction Remaining of Various Photocatalysts (a) 0.4 wt% GO-Bi_2WO_6 (b) 0.8 wt% GO-Bi_2WO_6 (c) 1.2 wt% GO-Bi_2WO_6 (d) 1.6 wt% GO-Bi_2WO_6

The comparison shows the optimum ratio was 1.2 wt%. Under this condition, almost all RhB was degraded after 1.5 hours of visible light irradiation. From 0.4 wt% to 1.2 wt%, the greater the GO content, the greater the degradation efficiency. This indicates to decompose organic compounds, more GO is needed to impede recombination of

electron-hole pair. However, when GO contents is greater than 1.2 wt%, degradation efficiency lowered, which shows that excessive GO will reduce the catalytic efficiency by decreasing effective absorption of light. While the optimum ratio may be around 1.2 wt%, it may not be the exactly 1.2 wt%; it is only the best result from this study, more ratio-response experiments must be done further to narrow down the actual optimal ratio.

4.3.3 Comparison from the Perspective of Photodegradation Kinetics

The Langmuir adsorption isotherm model is used to describe liquid-solid-phase adsorption, which is the sorption of aqueous compounds onto a solid phase (Kumar et al., 2008; Limousin et al., 2007). The mechanistic model assumes the adsorbed layer is one molecule in thickness (monolayer), which is adsorbed over an uniform and flat adsorbent surface (i.e. a photocatalyst) at a constant temperature (Kumar et al., 2008; Vijayaraghavan et al., 2006). The adsorption only occurs at a fixed number of localized positions on the surface, and there are no interactions and steric hindrance between adsorbed molecules or adjacent sites (Vijayaraghavan et al., 2006; Foo et al., 2010). Also, there is no transmigration of the adsorbate on the surface plane (Vijayaraghavan et al., 2006; Pérez-Marín et al., 2007). The distribution of the compound between the liquid phase and solid phase is controlled by the equilibrium constant (Kumar et al., 2008). At equilibrium conditions, the rate of adsorption and the rate of desorption are equivalent (Kumar et al., 2008). The Langmuir equation is:

$$q_e = \frac{q_m K_L C_e}{1 + K_L C_e}$$

Where q_m stands for the monolayer capacity of adsorption (mg/g). K_L is a constant representing the affinity of the binding sites (L/mg). They are the two Langmuir isotherm constants which will greatly impact the experimental conclusions and can be determined by linear regression equation optimization (Kumar et al., 2008; Limousin et al., 2007).

The linear form of the Langmuir-Hinshelwood expression is:

$$\frac{1}{q_e} = \left(\frac{1}{K_L q_m}\right)\frac{1}{C_e} + \left(\frac{1}{q_m}\right)$$

When $1/q_e$ is plotted against $1/C_e$. The slope of the plot is $1/K_L q_m$, and the intercept of the plot is $1/q_m$.

When initial concentration $C_0 << 10^{-3}$ mol/L, the Langmuir-Hinshelwood expression can be simplified to the following equation:

$$q_e = \ln\left(\frac{C_0}{C}\right) = k_r K t = k_1 t$$

Where k_1 stands for the pseudo-first order degradation rate constant (min^{-1}). K is the equilibrium constant (L/mg). And k_r is the limiting constant of a reaction at the maximum coverage (mg/(L·min)).

Removal efficiency can be expressed by the content remaining, using the equation $(Abs_0 - Abs)/ Abs_0 = (C_0-C)/C_0$, we get $(C_0-C)/C_0$ of each time. This produces the following equation:

$$\eta = (C_0-C)/C_0 \times 100\%$$

Where Abs_0 stands for the absorbance before degradation, Abs is the absorbance at the end of the degradation process. C_0 stands for the initial concentration (ppm). C is the concentration of dye solution after degradation (ppm).

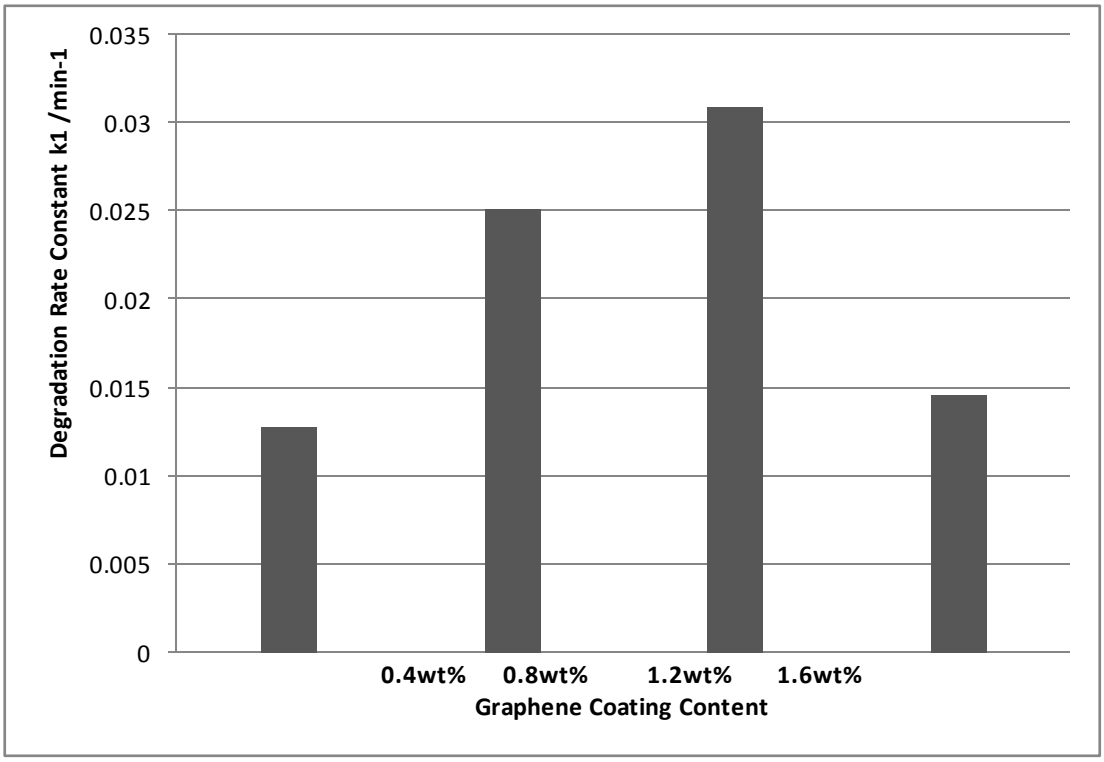

Figure 4- Degradation Rate Constant of Various Photocatalysts

(a) 0.4 wt% GO-Bi_2WO_6 (b) 0.8 wt% GO-Bi_2WO_6 (c) 1.2 wt% GO-Bi_2WO_6 (d) 1.6wt% GO-Bi_2WO_6

Table 1-Removal Efficiency of Various Photocatalysts Samples

(a) 0.4 wt% GO-Bi_2WO_6 (b) 0.8 wt% GO-Bi_2WO_6 (c) 1.2 wt% GO-Bi_2WO_6 (d) 1.6wt% GO-Bi_2WO_6

Removal efficiency				
content wt%	0.4	0.8	1.2	1.6
$(C_0-C)/C_0$	0.6844	0.8957	0.9382	0.7317

Figure 4 shows the degradation rate constant of various photocatalysts. The result is the same as in Figure 3. 1.2 wt% GO-Bi_2WO_6 is the one with the highest removal efficiency, which provides support for the result from a kinetic perspective. Table 1 demonstrates the removal efficiency of 1.2 wt% GO-Bi_2WO_6 is almost 1.5 times greater than that of the 0.4 wt% GO-Bi_2WO_6, which will improve the overall degradation efficiency and shorten the reaction time.

4.3.4 UV-Vis Diffuse Spectral Analysis

A UV-vis spectrophotometer was used to measure the retention concentrations of RhB solutions. For each absorption process, solution samples were taken every 10 min. Solid catalysts and dye solutions were separated by centrifugation. By monitoring the absorbance of the residual dye solution at its wavelength of maximum absorbance (λ_{max}=552nm), concentrations of RhB were calculated. The current dye absorption amount q_t was calculated from eq.1 (Ge et al., 2008).

$$q_t = \frac{V(C_0 - C_t)}{W} \quad (1)$$

When reaching equilibrium, $q_t = q_e$ $C_t = C_e$; the amount of sorbed dye, q_e was calculated from eq.2.

$$q_e = \frac{V(C_0 - C_e)}{W} \quad (2)$$

C_0 stands for initial concentration (mg/L); C_t current concentration (mg/L); C_e is equilibrium concentrations of dye solution (mg/L). V the volume of the solution (L), W the mass of adsorbent (g) (Wang et al., 2012).

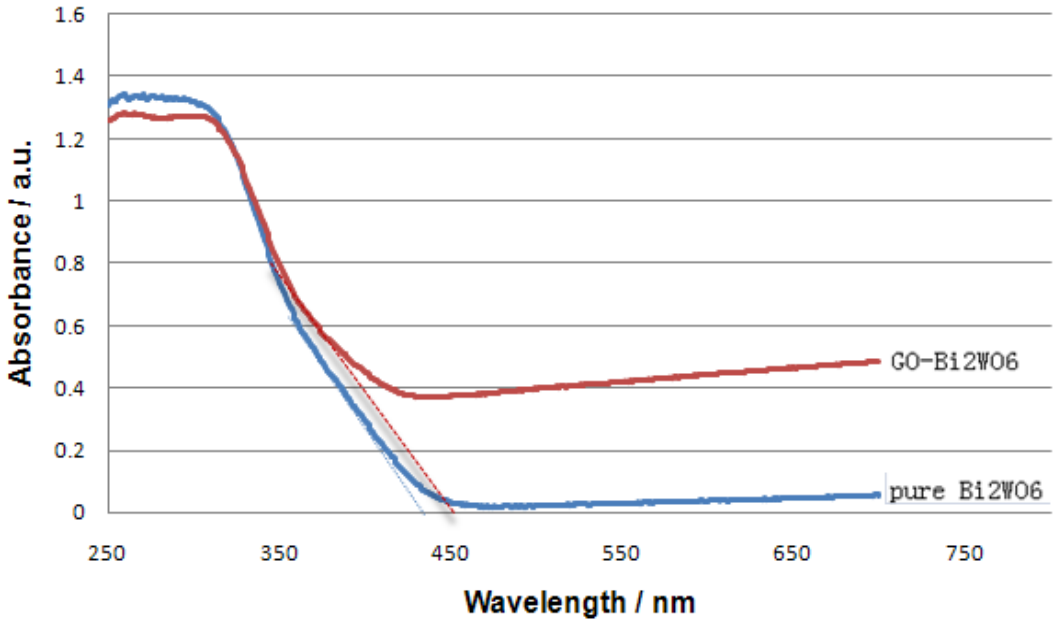

Figure 5- UV-Vis Diffused Reflectance Spectra of GO-Bi_2WO_6 and Pure Bi_2WO_6

The UV-Vis diffuse reflectance spectra of GO-Bi_2WO_6 and pure Bi_2WO_6. The absorbance wavelength increased after modification by GO (Figure 5). The band gap energy was calculated from the eq. 3.

$$\lambda = 1240/\mathrm{Eg} \quad (3)$$

Where λ stands for the maximum absorbed wavelength (nm) and Eg stands for the band gap energy (eV).

$$\lambda_{Bi2WO6} = 440\mathrm{nm} \Rightarrow \mathrm{Eg} = 2.81\mathrm{eV}$$

$$\lambda_{GO\text{-}Bi2WO6} = 460\mathrm{nm} \Rightarrow \mathrm{Eg} = 2.69\mathrm{eV}$$

After graphene oxide addition, wavelength increased so that band gap energy decreased, resulting in greater degradation efficiency.

The response range of GO is in the ultraviolet area. Bi_2WO_6 irradiation causes, some of the Bi^{3+} in Bi_2WO_6 to deoxidize into Bi^{+} (Ma et al., 2012). GO facilitates this

process by increasing the wavelength required to deoxidize bismuth. In turn, the generation of Bi^{+} nanoparticles enhances the response of GO-Bi_2WO_6 under visible light irradiation due to surface plasma resonance effect.

4.4 Optimize the Catalytic Performance

4.4.1 Operating Parameters: Catalyst Dosage

The effect of different dosages of GO/Bi_2WO_6 on the photocatalytic degradation of RhB was studied (Figure 6). The concentration of RhB was kept at 10 ppm, and the dosage of GO/Bi_2WO_6 varied from 0.5 g/L to 6 g/L. All the tests were done at pH 7 and 20°C.

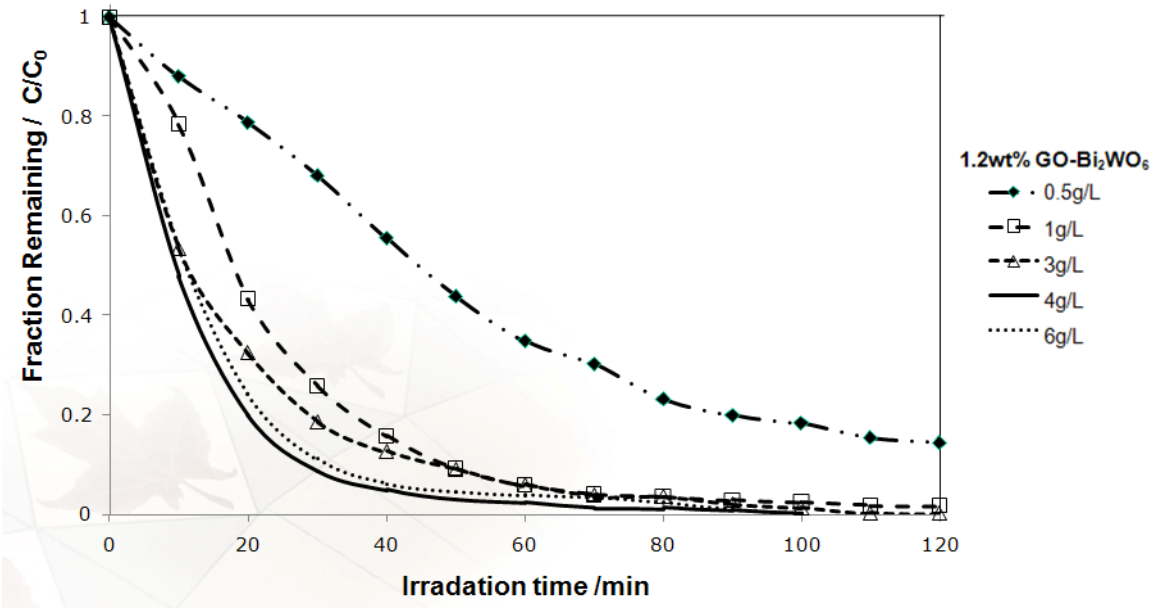

Figure 6- Fraction Remaining of Different Catalysts Dosage (1.2 wt% GO-Bi_2WO_6) (a) 0.5g/L (b) 1g/L (c) 3g/L (d) 4g/L (e) 6g/L

Degradation efficiency was the greatest when the catalyst dosage was at 4g/L. Degradation rate constant reached almost zero after two hours of visible light irradiation. From 0.5g/L to 4g/L, degradation efficiency increased as dosage increased. Decomposing organic compounds requires active sites to produce more hydroxyl radicals, which is why degradation efficiency increase as the number of active sites increase. However, when dosage rises above 4g/L, degradation efficiency becomes lower. GO dispersion is black, resulting in increased of light scattering and decreased of light penetration.

The degradation efficiency in the beginning was much higher than after 40 min, the activity of the catalyst gradually decreased and color faded more slowly (Figure 6). The reasons for this phenomenon will be discussed as follows.

The reaction solution became more viscous as catalysis proceeded, which made it harder for solids to separate from the liquid. Colloid molecules may have been blocking the pores of the catalyst, weakening the catalytic activity (Khan et al., 2003). Intermediates molecules produced during in the degradation of RhB may also have been clogging the pores of the catalyst, decreasing its activity.

Also, it could be that the intermediates are colourless (or have different and unknown colours) and thus, catalyst breaking down an intermediate would not be detected using this colorimetric assay.

4.4.2 Operating Parameters: pH

In addition to the catalyst dosage, another important factor affecting catalytic performance is the pH of the solution (Wang et al., 2012; Ma et al., 2013). The influences of pH of the RhB solution on the fraction remaining was investigated. All the tests were done with a catalyst dosage of 1g/L, temperature at 20 ℃ and initial concentration of 10 ppm (Figure 7).

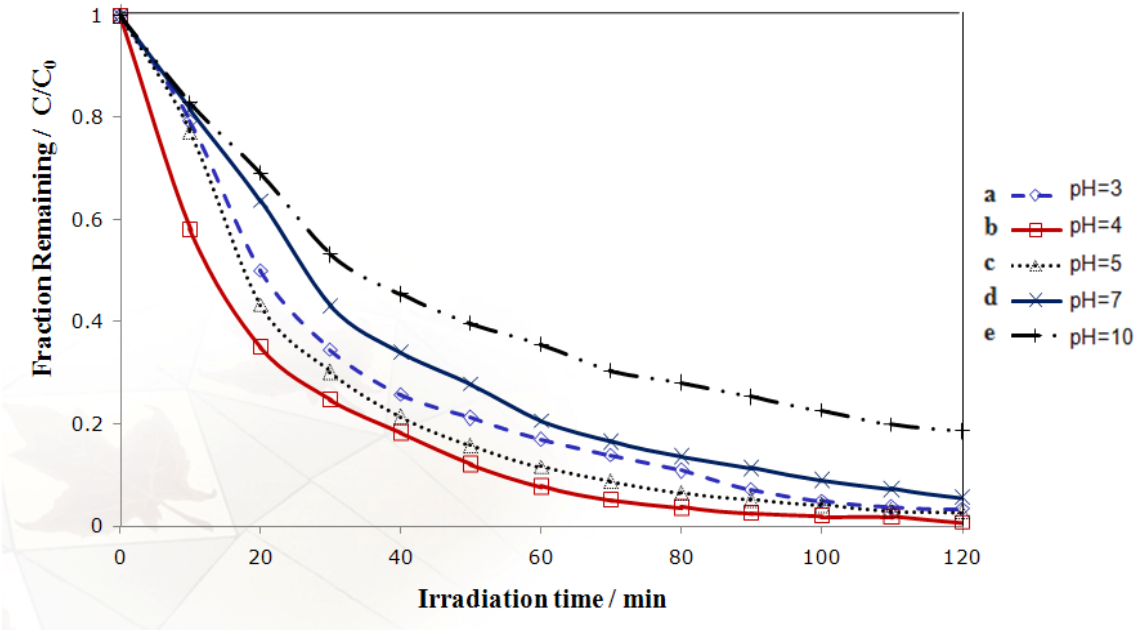

Figure 7- Fraction Remaining under Different Initial pH Value

(1.2 wt% GO-Bi_2WO_6) (a) pH=3 (b) pH=4 (c) pH=5 (d) pH=7 (e) pH=10

When the pH was equal to 4, a 10 ppm RhB solution was photodegraded by 1.2 wt% of GO-Bi_2WO_6 after 2 hours of visible light irradiation. Previous research indicated that pH influences the adsorption and degradation of dye pollutants, which influences the surface charge of photocatalyst (Wang et al., 2012; Ma et al., 2013). Moreover,

the initial pH value of the solution also affects the aggregation of the semiconductor photocatalyst and the band position of the photocatalyst in the solution.

4.4.3 Operating Parameters: Temperature

In addition to the catalyst dosage and pH value changes will affect the catalytic activity; temperature is another factor (Ma et al., 2013). All the tests were done with a catalyst dosage of 1g/L at pH 7 (Figure 8).

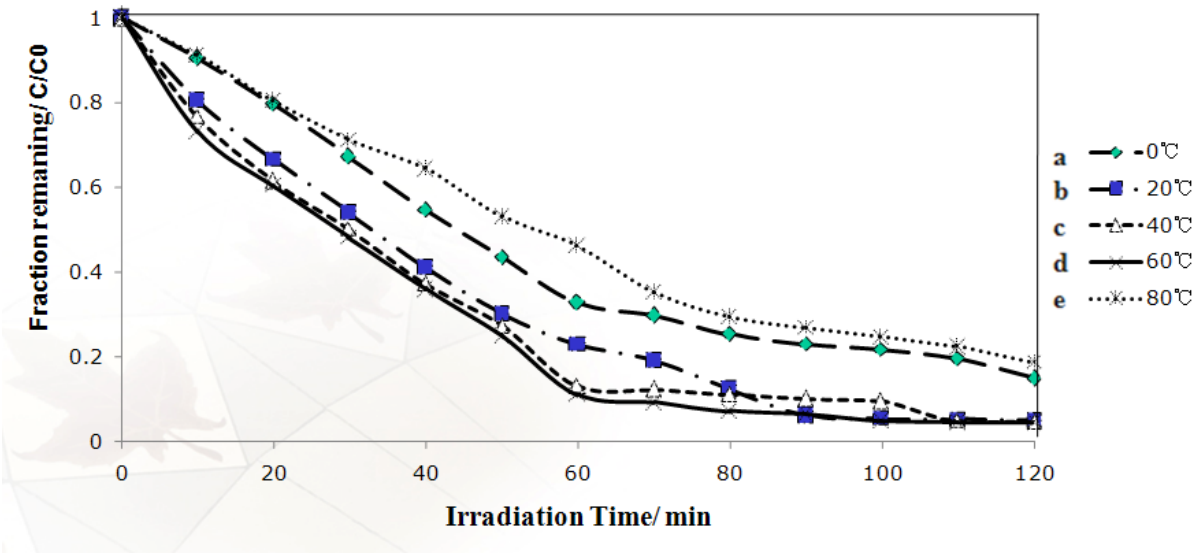

Figure 8- Fraction Remaining under Different Temperature

(1.2 wt% GO-Bi_2WO_6) (a) 0 ℃ (b) 20 ℃ (c) 40 ℃ (d) 60 ℃ (e) 80 ℃

Most photocatalytic reactions are not sensitive to minor variations in temperature. Most photocatalysis reactions can operate at room temperature without heating from outside sources due to the photonic activation. The true activation energy (Et) is nil,

while the apparent activation energy (Ea) is very small with a medium temperature range from 20 ^{o}C to 60 ^{o}C. When the reaction temperature is less than 20℃, the activity reduces, and (Ea) tends to heat of adsorption of the products. When the reaction temperature increases above 60 ^{o}C, high-temperature favors the recombination of charge carriers, and desorption of adsorbed reactant species happens. So the optimum value of reaction temperature is between 20 ℃ and 60 ℃. This also explains why solar devices require temperature controller.

4.5 Repeatability

Precision is measured by making repeat measurements on one sample under specific conditions. Repeatability is defined as replicate measurements are made in one laboratory, by the same analyst, using the same equipment over a short term (Leinonen et al., 2006). The repeatability tests were done with a catalyst dosage of 1g/L, at pH 7 and 20℃.

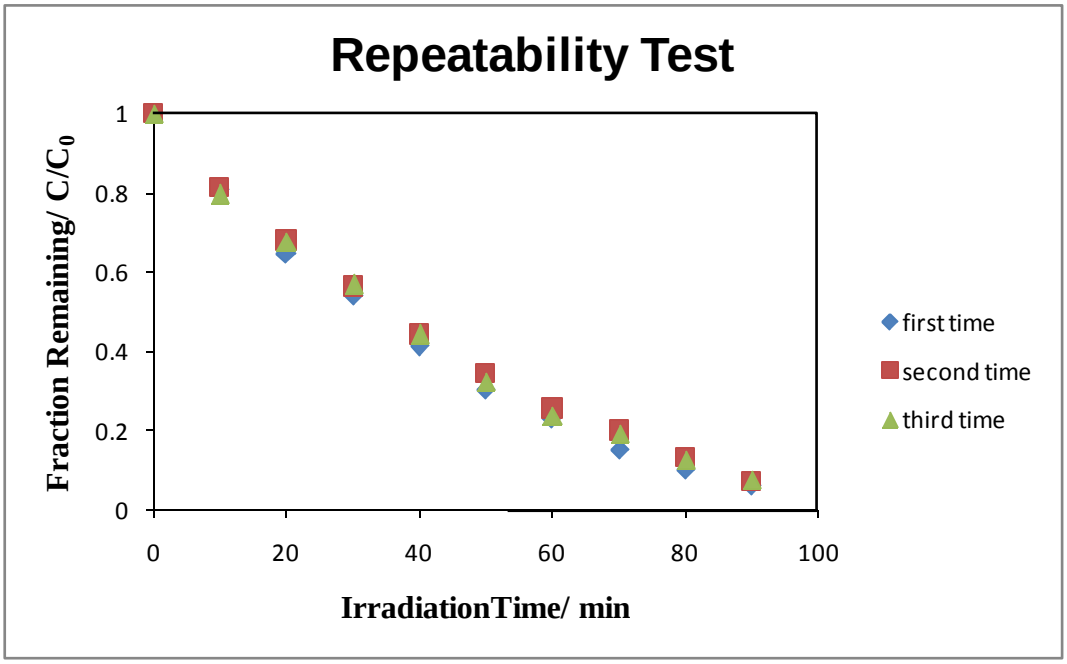

Figure 9- Repeatability test

The activity tests were repeated three times to ensure accuracy and precision within experiments. The result in Figure 9 confirms that the experimental operations are accurate and can be trusted. The experiment can also be repeated to obtain the same conclusion.

Table 2-Removal Efficiency of Repeatability Test

Removal efficiency			
	First time	Second time	Third time
$(C_0-C)/C_0$	0.9382	0.9264	0.9225

Table 2 confirms that the experimental operations are accurate for kinetics (removal efficiency). The experiment can be operated to get the repeatable conclusion.

4.6 Conclusion

GO-Bi_2WO_6 composite photocatalysts with different GO contents were successfully prepared using a template free hydrothermal reaction. Photocatalytic activity was studied by degradation of RhB. The photocatalytic activity of GO-Bi_2WO_6 was greatly enhanced compared to that of pure Bi_2WO_6 because of the synergetic effect between the conductive material and semiconductor. 1.2 wt% is the optimum modification ratio of GO to Bi_2WO_6. Using UV-vis diffraction to measure the band gap energy explains the enhancement of catalytic properties of the photocatalyst. This photocatalyst showed excellent photocatalytic performance under visible light irradiation. The activity of GO-Bi_2WO_6 was found to be a function of photocatalyst dosage, initial pH value of solution and temperature. The activity shows best when photocatalyst dosage reaches 4 g/L, initial pH 4 and 60 ℃. Each test was done in triplicate to guarantee the accuracy and repeatability of the photocatalysts.

4.7 References

Xiang, Q., Yu, J., & Jaroniec, M. (2012). Graphene-based semiconductor photocatalysts. *Chemical Society Reviews*, *41*(2), 782-796.

Zhang, J., Huang, Z. H., Xu, Y., & Kang, F. (2013). Hydrothermal Synthesis of Graphene/Bi_2WO_6 Composite with High Adsorptivity and Photoactivity for Azo Dyes. *Journal of the American Ceramic Society*, *96*(5), 1562-1569.

Gao, E., Wang, W., Shang, M., & Xu, J. (2011). Synthesis and enhanced photocatalytic performance of graphene-Bi_2WO_6 composite. *Physical Chemistry Chemical Physics*, *13*(7), 2887-2893.

Kumar, K. V., Porkodi, K., & Rocha, A. F. (2008). Langmuir–Hinshelwood kinetics–a theoretical study. *Catalysis Communications*, *9*(1), 82-84.

Foo, 5. 5. K., & Hameed, B. H. (2010). Insights into the modeling of adsorption isotherm systems. *Chemical Engineering Journal*, *156*(1), 2-10.

Limousin, G., Gaudet, J. P., Charlet, L., Szenknect, S., Barthes, V., & Krimissa, M. (2007). Sorption isotherms: a review on physical bases, modeling and measurement. *Applied Geochemistry*, *22*(2), 249-275.

Vijayaraghavan, K., Padmesh, T. V. N., Palanivelu, K., & Velan, M. (2006). Biosorption of nickel (II) ions onto< i> Sargassum wightii</i>: Application of two-parameter and three-parameter isotherm models. *Journal of Hazardous Materials*, *133*(1), 304-308.

Pérez-Marín, A. B., Zapata, V. M., Ortuno, J. F., Aguilar, M., Sáez, J., & Lloréns, M. (2007). Removal of cadmium from aqueous solutions by adsorption onto orange waste. *Journal of Hazardous Materials*, *139*(1), 122-131.

Ge, L. (2008). Synthesis and characterization of novel visible-light-driven Pd/$BiVO_4$ composite photocatalysts. *Materials Letters*, *62*(6), 926-928.

Wang, D., Xue, G., Zhen, Y., Fu, F., & Li, D. (2012). Monodispersed Ag nanoparticles loaded on the surface of spherical Bi_2WO_6 nanoarchitectures with enhanced photocatalytic activities. *Journal of Materials Chemistry*, *22*(11), 4751-4758.

Ma, H., Shen, J., Shi, M., Lu, X., Li, Z., Long, Y., ... & Ye, M. (2012). Significant enhanced performance for Rhodamine B, phenol and Cr (VI) removal by Bi_2WO_6 nancomposites via reduced graphene oxide modification. *Applied Catalysis B: Environmental*, *121*, 198-205.

Khan, S. U., Al-Shahry, M., & Ingler, W. B. (2003). Response to Comments on" Efficient Photochemical Water Splitting by a Chemically Modified n-TiO_2". *Science*, *301*(5640), 1673-1673.

Leinonen, J., Laakkonen, E., & Laatikainen, L. (2006). Repeatability (test‐retest variability) of refractive error measurement in clinical settings. *Acta Ophthalmologica Scandinavica*, *84*(4), 532-536.

Chapter 5-Conclusions and Recommendations

5.1 Summary and Conclusions

Based on this study, it can be inferred that GO-Bi_2WO_6 shows promising results for applications in solar-activated wastewater treatments. The Bi_2WO_6 composite photocatalyst was successfully prepared via a hydrothermal reaction and was incorporated into GO. The photocatalytic activity of the prepared samples was evaluated under different experimental and operating conditions. It was discovered that the photocatalytic activity of GO-Bi_2WO_6 is greatly enhanced compared to pure Bi_2WO_6, and 1.2wt% is the optimum ratio. By XRD, SEM and STEM observations, it was found that the participation of GO did not affect the crystal lattice structure of the Bi_2WO_6 photocatalyst. Furthermore, optimizing catalyst dosage, temperature and pH can improve the removal efficiency of RhB. The photocatalyst prepared using the described synthesis method is also found to be repeatable. In summary, it was demonstrated that Bi_2WO_6 photocatalytic activity was enhanced using GO cooperation. This modified photocatalyst is promising to implement in actual wastewater treatment.

5.2 Recommendations for Future Work

From this study, a series of problems and possible solutions were encountered, all of which shows that the new photocatalyst cannot be used in the actual production and application in its current state. However, the following recommendations described in this thesis offer a substantial endorsement for further research and commercialization of the photocatalyst for wastewater treatment systems.

In the current research, we focused on the hydrothermal method of synthesizing GO-Bi_2WO_6 because it is the most efficient method reported so far. However, other methods (such as the solvothermal and ionic liquid method) may have a yield far better results.

GO was the only material studied in the experiment; reduced GO and graphene can be investigated. Other noble metals (Pt, Ru and Au, etc.) can be loaded on Bi_2WO_6 to see if they will improve the photocatalysis.

RhB inherently exists sensitization to visible light. Therefore, using RhB as the only model pollutant to evaluate the activity cannot precisely measure the property of the catalyst. As a further object of degradation, one should choose a non-visible light absorbing pollutant such as phenol.

Photocatalytic activities should be conducted under the real sun or solar simulated irradiation to confirm the real life practical applicability of the photocatalyst.